Esther Garcia Merino
Licenciada em Fisica

Dielectric Study of Triton X100: a Glass-forming liquid

Dissertação para obtenção do grau de mestre em Engenharia de Materiais

Orientadora: Drª Natalia Correia, DQ-FCT/UNL
Orientadora: Prof. Drª Madalena Andrade Dionisio, DQ-FCT/UNL
Co-orientador: Prof. Dr. João Paulo Borges, DCM-FCT/UNL

Júri:

Presidente: Prof. Dr. João Pedro Botelho Veiga
Arguente(s): Prof. Dr. Carlos Jorge Mariano Dias
Vogal(ais): Drª Natalia Correia, DQ-FCT/UNL
Prof. Drª Madalena Andrade Dionisio
Prof. Dr. João Paulo Borges

FACULDADE DE CIÊNCIAS E TECNOLOGIA
UNIVERSIDADE NOVA DE LISBOA

February, 2012

Dielectric Study of Triton X100: a Glass-forming liquid

RESUMO

O presente trabalho teve como objectivo principal efectuar um estudo exaustivo sobre a mobilidade molecular de um líquido formador de vidro e estudar a sua resposta quando se encontra sujeito a confinamento em materiais inorgânicos nanoporosos.

O líquido seleccionado, Triton X100, caracteriza-se por apresentar elevada resposta dieléctrica e uma marcada tendência para cristalizar quer a partir do estado líquido quer do estado vítreo, embora seja possível encontrar condições em que a cristalização é evitada e o material entra num estado de líquido sobre-arrefecido. Isto permitiu-nos estudar a sua mobilidade no estado líquido, líquido sobrearrefecido, vítreo e durante a cristalização e investigar as transformações de fase que ocorrem sob diferentes historias termicas.

Para obter uma visão ainda mais global, estudos de cristalização isotérmica a diferentes temperaturas e a partir de ambos os estados, vítreo e fundido, foram efectuados e monitorizados em tempo real por Espectroscopia de Relaxação Dielectrica (DRS). Esta técnica permitiu obter informação sobre a influência da cristalização sobre a mobilidade da fase amorfa que permanece.

Motivados pelo conhecimento recente de que mobilidade molecular e as transformações de fase podem ser significativamente alteradas quando o líquido está confinado a dimensões na ordem nanométrica, avaliou-se a dinâmica molecular do Triton X100 confinado em materiais mesoporosos (SBA-15 e MCM-41; tamanho de poro respectivamente, 5.7 e 3.4 nm). Este estudo revelou que o confinamento em SBA-15 é uma estratégia eficaz para evitar a cristalização do Triton X100 independentemente da história térmica.

A técnica principal utilizada foi a Espectroscopia de Relaxação Dieléctrica (DRS) que permitiu fazer um estudo da mobilidade molecular num largo intervalo de frequências (10^{-2} – 10^{6} Hz). Como técnicas complementares utilizaram-se a Calorimetria Diferencial de Varrimento (DSC) e Microscopia Óptica de Luz Polarizada (POM).

Do trabalho efectuado nos estudos de cristalização resultou um artigo publicado na revista *Journal of Physical Chemistry B* **2011,** 115, (43), 12336-12347.

Palavras-Chave: Espectroscopia Dieléctrica, Triton X100, Cristalização, Transição vítrea, Confinamento.

ABSTRACT

The main purpose of this work was to realize an exhaustive study on the molecular mobility of a glass-forming liquid and evaluate the influence of thermal treatment in the phase transformations undergone by the material. It was also our goal to investigate it response when subjected to confinement in nano-porous inorganic materials.

The liquid selected, Triton X100, is characterized by a high dielectric response and a high tendency to crystallize by coming from both molten and glassy states. However, it is possible to find the conditions under which crystallization is avoided and the material enters in the supercooled liquid state. This allowed us to study the molecular mobility in the liquid, supercooled liquid, glassy states and as well as the crystallization and investigate temperature driven phase transformations.

To get a further insight in the crystallization behaviour, isothermal crystallization at different temperatures and from both glassy and molten states was promoted and monitored in real-time by Dielectric Spectroscopy Relaxation. This study gave information about the influence of the crystallization on the remaining amorphous phase.

Motivated by the recent knowledge that molecular mobility and phases transformations can be significantly altered when a glass-forming liquid is confined in the nanometer scale, the molecular dynamics of the Triton X100 was evaluated when confined in mesoporous materials (SBA-15 and MCM-41; pore size, respectively, 5.7 and 3.4 nm). This study revealed that the confinement in SBA-15 is an effective strategy to avoid the crystallization of the Triton X100 independently of the thermal history.

Dielectric Spectroscopy Relaxation (DRS) was the main technique used to obtain detailed information about the molecular mobility in a wide range of frequencies (10^{-2} – 10^{6} Hz). As complementary techniques Differential Scanning Calorimetric (DSC) and polarized Optical Microscopy (POM) were used.

Some of the results have been published in the *Journal of Physical Chemistry B* **2011,** 115, (43), 12336-12347.

Keywords: Dielectric Spectroscopy, Triton X100, Crystallization, Glass transition, Confinement.

GENERAL INDEX

FIGURE INDEX

Appendixes

TABLE INDEX

LIST OF SYMBOLS AND ABBREVIATIONS

Triton X100	TR100
T	Temperature
T_{cr}	Crystallization temperature
T_g	Glass transition temperature
T_m	Melting point temperature
f	Frequency
τ	Relaxation time
τ_∞	Pre-exponential factor
T_0	Vogel temperature
E_a	Activation energy
R	Ideal gas constant (8.3144621 $J \cdot K^{-1} \cdot mol^{-1}$)
$\xi(T)$	Cooperative length
t	Time
$E(t)$	Electric field
$D(t)$	Dielectric displacement
ε_0	Vacuum permittivity (8.854×10^{-12} $F \cdot m^{-1}$)
ε_∞	Instantaneous relative permittivity
ε_S	Permittivity at low frequency
$\Phi(t)$	Dielectric function
E_o	Field amplitude of electric field
ω	Angular frequency
ε^*	Dielectric permittivity (complex dielectric function)
P	Polarization
P_0	Polarization at moment of field removal
ε'	Real component of dielectric permittivity
ε''	Imaginary component of dielectric permittivity or dielectric loss
f_{max}	Maximum frequency
HN	Havriliak-Negami
$\Delta\varepsilon$	Dielectric strength
τ_{HD}	Relaxation time of HN function
β_{HD}, α_{HD}	Shape parameter of HN function
τ_0	d.c.-conductivity (d.c. :direct current)
μ_0	Permeability
g	Correlation factor

ΔH_m	Melting enthalpy
ΔH_{cr}	Crystallization enthalpy
χ_{cr}	Crystallinity degree
ε'_N	Normalized real permittivity
n	Avrami parameter
k	Crystallization rate constant
t_0	Induction time preceding crystallization

VFTH	Vogel-Fulcher-Tammann-Hesse
CCR	Cooperative Rearranging Regions
XRD	X-Ray Diffraction
TEM	Transmission Electron Microscopy
BET	Brunauer-Emmett-Teller
BJH	Barrett-Joyner-Halenda
DRS	Dielectric Relaxation Spectroscopy
DSC	Differencial Scanning Calorimetry
POM	Polarized Optical Microscopy
TGA	Thermo Gravimetric Analysis
ATR-FTIR	ATR-Fourier Transform Infrared

Chapter I: Introduction

Outline

The factors that govern the interconversion between amorphous and crystalline states for a glass-forming liquid and their stability are fundamental aspects of several areas of science and technology gaining special importance in pharmaceutical[1-3] and food industries. A study about the molecular mobility and the effect that the thermal treatment have in the glass transition for a glass former can help us to found factors that explain the conversion between the amorphous and crystalline forms.[1, 2, 4, 5] In this context, understanding key questions as under what conditions an amorphous leads to crystal formation and the relation between temperature, glass transition and crystallization pathways are particular interesting in the condensed-matter physics.[6]

Moreover, it is well known that the molecular behaviour of glass-forming liquids, polymers and liquid crystals are affected by confining it in nanoscaled geometries.[7-10] Dynamic experiments can prove that the molecular relaxation in a restricted geometry differs from the one of the bulk. This is called the confinement effect and may provide additional information on the dynamics of glass transition.

This work is mainly dedicated to characterise the molecular mobility of a glass-forming liquid and evaluate the influence of thermal treatment in the phase transformations undergone by the material. A study about the impact that the geometrical constraints have in the molecular mobility in the glass former is also presented.

The water-soluble, liquid surfactant Triton-X 100 with the molecular formula $C_{14}H_{22}O(C_2H_4O)_n$ (with n = 9~10), is our glass-forming liquid. This nonionic detergent is widely used in industrial and pharmaceutical formulations and in biological applications such as solubilisation of membrane proteins without losing their activity[11] and isolation of membrane rafts[12], and it also forms transparent microemulsions capable of dissolving both water and oil in relatively large amounts.[13] Due to the fact that it holds an high dielectric response and is able to prevent crystallization (melting) when rapidly cooled, it enables us to study molecular mobility in the following states: liquid, supercooled liquid and glassy states.

The Triton X100 has the ability to crystallize from both molten (melt-crystallization) and glassy (cold-crystallization) states, so isothermal crystallization was monitored on real time by dielectric relaxation spectroscopy (DRS) at a temperature nearly above the glass transition temperature ($T_{cr} \sim T_g+6$) between 1 Hz and 1 MHz. The usual way as dielectric spectroscopy is used to follow isothermal crystallization is through the reduction of the dielectric strength of the process associated with the dynamical glass transition, α-relaxation, either in polymers like PET[14], PLLA[15-17] and polycarbonate/poly(ε-caprolactone) blends[18], or low molecular weight materials.[19-21] To our knowledge such kind of studies have not been reported for neat Triton X-100; published results refer

mainly mixtures of triton X-100 with water where the dielectric behaviour of the neat material is studied at room temperature only in a frequency range from 10^6 to 10^{10} Hz.

The present work represents an additional contribution concerning crystallization behaviour of low molecular weight glass formers. Moreover, the kinetics of isothermal crystallizations will be analysed by the classical Avrami law[22-24] which, in a double logarithmic plot, linearizes the time dependence of the crystallinity degree. The parameters thus obtained are compared to those estimated from the direct fit to the normalized real dielectric permittivity.

Therefore, a sample of Triton x-100 impregnated in SBA-15 (nano-porous material host) is measured over a broad frequency range The result showed that the dynamical behaviour of the confined guest differs from the dynamical of the bulk state, a new relaxation, related with the molecules absorbed to the internal pore wall, the S-process, was found and the confined Triton X100 is in amorphous state at room temperature. In this case, the confinement emerges as a method of stabilizing the amorphous phase, which is mostly important in pharmaceutical activity.[7, 25, 26]

1.1 The glass transition and molecular mobility

A major aspect of the work developed in this thesis, concerns to molecular mobility of materials in the solid state, which is a main issue of the physics of condensed matter.

Glass transition is a universal phenomenon as it can be observed in organic[27], inorganic[28], polymeric[29] and metallic systems[30] and that plays an important role in life sciences.[31] The transition from the liquid to the glassy state is considered as one of the unresolved problems of condensed matter physics because it is not easy to explain under what conditions an ensemble of a few molecules starts to behave like a liquid.[6, 32, 33]

Mainly, when a liquid is cooled below its melting temperature, molecular motions slows down and if the liquid is cooled sufficiently fast and the crystallization is avoided, the liquid in such state is called supercooled. If the temperature continues to decrease, the intermolecular rearrangements are so slow that the liquid vitrifies becoming a glass (see figure 1.1). This evolution that dependent on the cooling rate is a kinetic phenomenon and not a thermodynamic transition. The glassy state is an out-of-equilibrium state in which the molecular mobility is mostly frozen but without long-range order.

The materials that circumvent crystallization undergoing vitrification upon further cooling are designated as **glass-former**s.[32, 34]

The transition between a disordered state with high molecular mobility (liquid) and an immobilized state with a similar structure (glass) take places in a broad temperature range but it is common to use the term glass transition temperature, T_g, to localize this temperature range. Normally, T_g is defined as the temperature where the characteristic molecular relaxation time becomes of the order of 100 seconds or the viscosity reaches the value of 10^{13} Poise. Its value will obviously depend the molecular

structure and on the ability of the material of forming a glass (thermal history, molecular weight, degree of crystallinity, confined…).

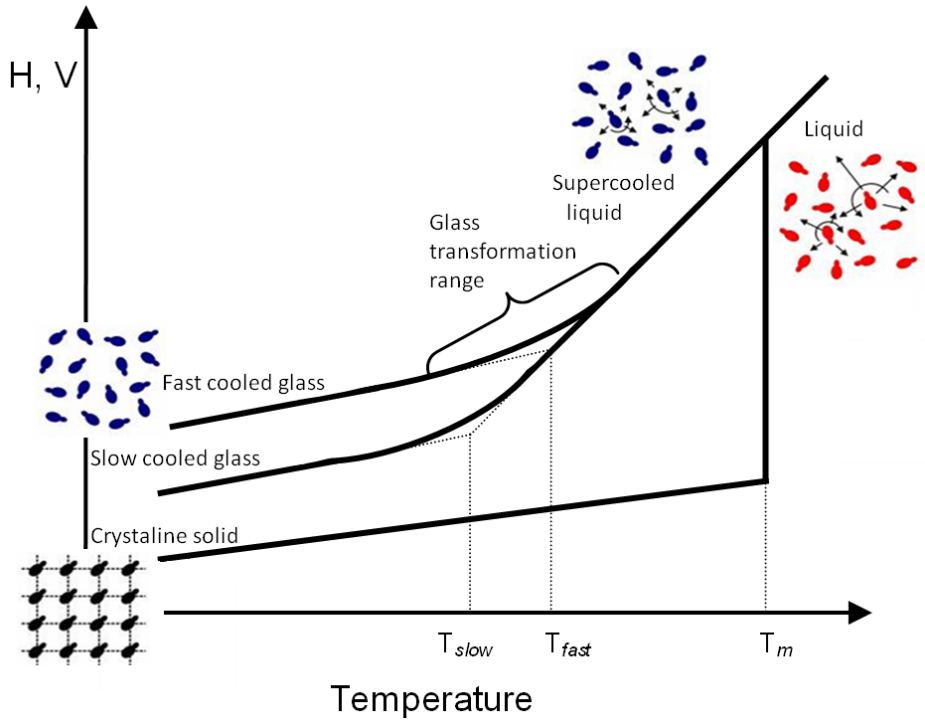

Figure 1.1 Schematic representation of the specific enthalpy (H) or volume (V) as a function of temperature for a liquid that can both, crystallize or vitrify in two different depending on the cooling rate. Adapted from [34] by Miriam Sousa.[35]

1.2 Dynamical glass transition: the different relaxation modes probed by dielectric relaxation spectroscopy

Understand the transition from the liquid to the glassy state and the continuous slowdown of the molecular dynamics when approaching the glass state is one of the problems that the condensed matter physics try to explain. Consequently, many recent theoretical and experimental studies have focused on the investigation of the relaxation dynamics of glass-forming liquids.[36, 37] To characterize the typical dynamics of the structural rearrangement of the molecules constituting the glass, dielectric spectroscopy relaxation has been use in this work.

The conformational mobility, i.e. molecular rearrangements able to change the spatial disposition of the molecules, determines the behaviour of the material in the liquid state. Upon cooling, when the viscosity increase, the molecular mobility is continuously decreasing until the glass transition region is reached, where is becomes so reduced that the time available for intermolecular rearrangements becomes comparable to the time scale of the experiment, originating a structural state frozen-in for practical purposes. The slower the liquid is cooled, the longer the time available for configurational

sampling at each temperature, and hence the lower the temperature it can achieve before falling out of liquid-state equilibrium, which means a lower T_g.[35, 38, 39]

The dynamic in liquids involves a series of relaxation processes that goes from very local motions (γ, δ, β… processes) or secondary relaxations to segmental mobility exhibiting cooperativity (α relaxation), corresponding to the dynamic glass transition.

1.2.1 α-relaxation

The α relaxation process takes place in amorphous polymers and low molecular weight glass-formers in the liquid state, at temperature above the glass transition temperature. The application of an electric field to the l glass-formers in the liquid state leads to the rearrangements cooperative of the material which means that a specific unit moves together with its environment.[39, 40] Usually it is a "strong" relaxation, characterized by a broad range of characteristic (over many orders of magnitude).

In dielectric experiments performed at a given frequency, the α relaxation takes place in response to the dielectric field reaching a value in the order of $(2\pi f)^{-1}$ seconds, where f is the frequency of the applied oscillating electrical field.

One of the striking features of the alpha relaxation is the non-Arrhenius dependence of the characteristic times with temperature due to the abrupt increase of the relaxation time with the temperature decrease.

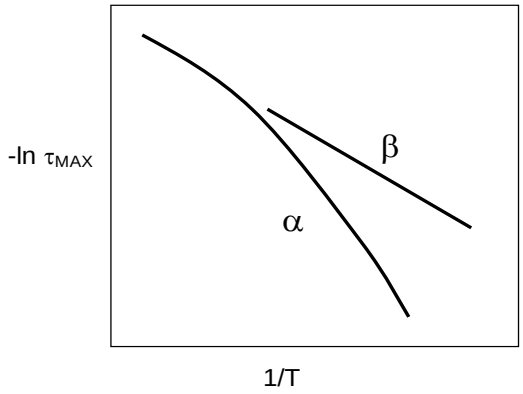

Figure 1.2 Relaxation map of time (or frequency) variation dependent with temperature for the α and β relaxation.

This relaxation time dependence could be described by the Vogel-Fulcher-Tammann-Hesse equation [41-43](VFTH):

$$\tau(T) = \tau_\infty \exp\left(\frac{A}{T-T_0}\right), T_0 < T_g \qquad \text{Equation 1.1}$$

where τ_∞ is of the order of 10^{-13} s and T_0 is the Vogel temperature, interpreted as the glass transition temperature of an ideal glass, wich is generaly 30-70 K below T_g. [44]

The activation energy is given by:

$$E_a = R\frac{dln\tau}{d(1/T)}$$ Equation 1.2

where R is the ideal gas constant and increases dramatically as we are approaching T_g. However, this is not a real activation energy, since it not refers to a true activation barrier.[44, 45]

There are three different ways to rationalize the phenomenon of the glass transition, in terms of free volume, kinetically or thermodynamically, may at first appear to be distinct but in fact they just analyze three aspects of the same phenomenon. Adam and Gibbs attempted to unify these 3 theories of the glass transition by proposing the concept of "cooperative rearranging regions" (CCR).[46] This theory defines that the changes in the relaxation time in the glass-transition region could be interpreted as a change in the length scale of the segmental motions that are increasing as the temperature decreases. The Adam-Gibbs theory establishes a link between configurational entropy and the molecular relaxation time, showing that upon vitrification a decrease in the number of available configurations to the system is associated to a remarkable increase in the characteristic relaxation times. The molecular motions in a liquid are characterized by an increase in the size of CRR or, in other words, an increase in the cooperative length, ξ(T)(see figure 1.3, adapted from reference [47]).

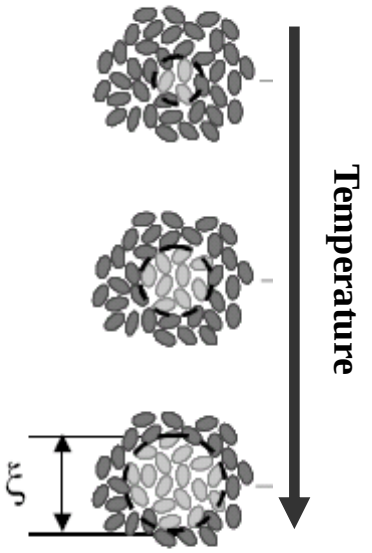

Figure 1.3 Schematic representation for the increasing cooperative region with decreasing T near the glass transition.

1.2.2 Secondary relaxations

Secondary relaxations are associated with more localized mobility and usually emerge with less intensity in DRS signals. All secondary relaxations are thermally activated processes meaning that the temperature dependence of their relaxation times is Arrhenius type (see linear representation in figure 1.2).

$$\tau(T) = \tau_\infty exp[E_a/RT]$$ Equation 1.3

where τ_∞ is the relaxation time at infinite temperature, and E_a is the activation energy representing the potential barrier resisting the molecular rearrangement.[48]

Below T_g, in the glassy state, two types of dynamical processes are observed: localized motions that are the origin of the secondary relaxation processes and a very slow dynamic process due to structural recovery as evidenced by physical ageing processes.[40]

Nevertheless, the molecular origin of the β relaxation is not completely understood, being observed in a variety of materials, including polymers, glass-forming liquids and rigid molecular glasses.

Goldstein and Johari proposed a near-universal feature of the amorphous state, called the β_{JG} process.[49] In this model, the amorphous state is characterized by the motion of the molecules as a whole but it´s not the only model using to try to explain the origin of the β process, another authors interprets the presence of the observed secondary relaxation as the result of some specific molecular motion.[50-52] Frequently, at the high-frequency side of the β-relaxation, an additional process is detected due to even more local dynamics, designated γ-process.[53]

1.3 Crystallization: molecular mobility in semicrystalline materials

When the crystallization of a glass former is not avoided, it is possible to find conditions in which it occurs simultaneously with vitrification.[54] In this case, in the final product, the crystalline and the amorphous phase will coexist and the molecular mobility of the latter can be distinct from the mobility of the completely amorphous material.[39]

The presence of crystallinity may affect the molecular dynamics in two main ways:[39, 55]

i) A fraction of the amorphous phase may be partially confined within the crystalline lamellae. Therefore, the chains will have a constrained mobility and we may expect serious changes in the glass transition dynamics. This means that the glass transition in semi-crystalline polymers depends on the crystalline fraction and also on its microstructure.

ii) The existence of crystalline structures may introduce new relaxation processes involving motions within the crystallites, or loss processes due to mobility between crystalline regions. In this case, it is possible to induce a high degree of crystallinity during the measurement which will produce some changes in the glass transition dynamics.

1.4 Dynamics under confinement

Investigate the effects induced by confinement on glass transition for the glass-forming liquids in confining geometries can provide additional information about the dynamics of glass transition and may help to check some of the different theories and models proposed.[32, 33]

The molecular dynamics of molecules confined to nanoporous hosts results from a balance between surface and confinement effects.[10] When the glass transition,T_g, tends to decrease, the interaction between the glass former guest and the matrix is low and the mobility of the guest is enhanced relative to bulk.[10, 56] This is called in literature, the confinement effect.[10] If the value of T_g increases, molecular dynamics of the confined guest is not only determined by confinement, but also by surface interactions between the host and the guest molecules.[9, 57] Additional effects to take into account are phase transition and ordering that could involve the formation of a surface layer with a partial ordering close to the wall of the host.[35, 40]

These effects can produce interesting changes in the molecular dynamics properties and influence the thermodynamic properties of the confined phase.[58] In real experiments, the molecular dynamics in confining space is in general determined by the counterbalance between surface and confinement effects[56], so that it is very difficult confirm or disprove bulk characteristic lengths.[40, 59] It is evident that this counterbalance also must depend sensitively on the type of confined molecules (glass-forming organic liquids, polymers, liquid crystals, proteins, lipids and more recently ionic liquids), on the properties of the (inner and outer) surfaces (wetting, non-wetting) and on the architecture of the molecules with respect to the walls (grafted, layered or amorphous systems).[10, 40]

1.5 Dielectric relaxation spectroscopy

Dielectric spectroscopy is one of the most commonly used techniques for the investigation of the dynamic response of glass-forming materials. DRS is a suitable tool for monitoring molecular mobility covering an extended dynamic range from 10^{-6} to 10^{12} Hz, and thus providing a source of information on the dynamics of bound dipoles and mobile charge carriers according with the properties of the molecular system.[44] Prerequisite, of course, is the presence of a dipolar moment.

Relaxation can be interpreted as a delayed response of the sample to an applied stimulus at a given instant. Therefore, dielectric relaxation comprises a dielectric material containing permanent dipoles as the system, an oscillating electric field as the stimulus, and a polarization as the response. The delayed polarization from the applied electric field is due to an irreversible loss of free energy in the form of heat, which is the main effect related with molecular dynamics.[35, 60]

When an electric field is applied across the faces of a parallel plate capacitor containing a dielectric (a material that restricts the flow of current), the atomic and molecular charges in the dielectric are displaced from their equilibrium positions and the material is said to be polarized. Different mechanisms of polarization can be induced in a dielectric material[61]: electronic polarization – which arises when electrons are displaced from the equilibrium position with respect to the atomic nucleus; atomic polarization – which arises when occurs a modification in the relative positions of atomic nuclei in a molecule or in an atomic network (movements like bending, twisting or stretching of molecules, slower than those from electronic polarization); orientation or dipolar polarization – observed only in materials with molecular or ionic dipole moments which results in a preferred dipole orientation in the direction of the electric field.

At this moment, it is important to emphasize that the time of response of the three types of polarization are very different: around 10^{-17} and 10^{-14} s for electronic, 10^{-13} to 10^{-12} s for atomic polarization, and between 10^{-5} e 10^{-12} s for orientational one.[35, 61]

Upon removal of the electric field, the electronic and atomic polarizations (also designed by induced polarization) disappear immediately. In contrast, the orientational polarization falls down slowly (comparatively to those ones). This lag is due to the internal friction of the material, and it depends on viscosity. Keeping this in mind, naturally arise the necessity of define a parameter that describes the polarization loss when the electric field is turned off. This parameter is the characteristic time, known by **relaxation time** (required time to polarization decreases a factor 1/*e* from its initial value).[39]

Dielectric relaxation spectroscopy is precisely based in the measure of this loss of polarization (*i.e.* dielectric relaxation) after removal of a sinusoidal electric field at a certain temperature. The way as these dipoles relax will be rationalized in terms of molecular mobility existing in the system.

Figure 1.5 illustrates the frequency location of the several mechanisms involved in the polarization, and intensity, height and width of the respective bands. Notice that atomic and electronic polarization mechanisms have fast, nearly instantaneous responses, characterized by sharp bands on the optical domain (UV-Vis and IR), whereas orientation/dipolar polarization have broader bands due to the resistance of the medium on the dipole's motion leading to slower responses.[60]

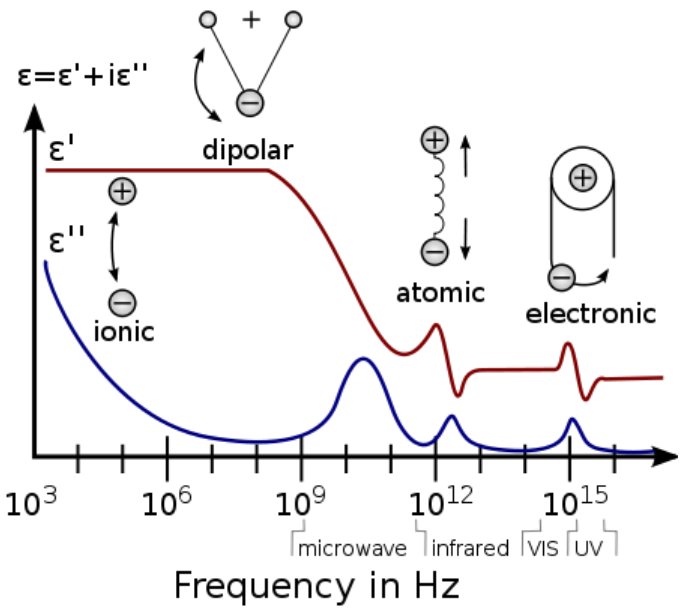

Figure 1.4 Frequency response of dielectric displacements that represent the polarization phenomena. Adapted from [62].

Dielectric relaxation spectroscopy is a particular case where the experiments are developed in the linear response regime. Here the stimulus is an electric field $E(t)$, and the response is the dielectric displacement $D(t)$. When the electric filed is static, the dielectric displacement resulting at $t = 0$ is:

$$D(t) = \varepsilon_0[\varepsilon_\infty + (\varepsilon_S - \varepsilon_\infty)\Phi(t)]E \qquad \text{Equation 1.4}$$

where ε_0 is the vacuum permittivity, ε_∞ is the permittivity of induced polarization and ε_S is the static permittivity. The first term represents the instantaneous response of dielectric material to the field, and

the second,$(\varepsilon_S-\varepsilon_\infty)\Phi(t)E$, is related to the slower response to dipolar polarization, including the dielectric function $\Phi(t)$, that describes the polarization response after switching off the electric field. The decrease of polarization after removing the electric field can be expressed by decay function, described by $\Phi(t)= 1- e^{-t/\tau}$.

If the applied electric field is variable, the variation in *D(t)* produced by the increment *dE* at *t=u* is:

$$D(t) = \varepsilon_0\varepsilon_\infty dE+\varepsilon_0(\varepsilon_S-\varepsilon_\infty)\Phi(t-u)dE \qquad \text{Equation 1.5}$$

With application of Boltzmann's principle, substituting $t' = t - u$, integrating and applying a harmonic electric $E(t) = E_0\exp(i\omega t)$, where ω is the angular frequency, the expression of the dielectric response obtained is:

$$\frac{D(t)}{\varepsilon_0 E(t)} = \varepsilon_\infty + (\varepsilon_S-\varepsilon_\infty)\int_0^\infty \exp(-i\omega t')\left[\frac{-d\Phi(t')}{d(t')}\right]dt' \qquad \text{Equation 1.6}$$

Where:

$$\frac{D(t)}{\varepsilon_0 E(t)} = \varepsilon^*(\omega) \qquad \text{Equation 1.7}$$

and the dependent of $\varepsilon^*$with the frequency is:

$$\frac{\varepsilon^*(\omega)-\varepsilon_\infty}{\varepsilon_0-\varepsilon_\infty} = \int_0^\infty \exp(-i\omega t')\left[\frac{-d\Phi(t')}{d(t')}\right]dt' \qquad \text{Equation 1.8}$$

Considering that relaxation increases linearly with the distance from equilibrium (Debye model)[63]:

$$\frac{dP(t)}{dt} = -\frac{P(t)}{\tau_D} \qquad \text{Equation 1.9}$$

where τ_D is a characteristic relaxation time and it is assumed that i) no interaction between the dipoles occurs, ii) only one process leads to equilibrium, and iii) all the dipoles are equivalent, i.e. all dipoles relax with only one relaxation time. The orientation polarization is given by $P(t) = P_0 exp^{-t/\tau}$ where P_0 is the value of the polarization at the moment of field removal. In this case $\Phi(t)$, in equation 1.8, is a function in the form of $k \cdot exp^{-t/\tau}$, which solution leads to the Debye dispersion equation:

$$\varepsilon^* = \varepsilon'(\omega) - i\varepsilon''(\omega) = \varepsilon_\infty + \frac{\varepsilon_S-\varepsilon_\infty}{1+i\omega\tau} = \left(\varepsilon_\infty + \frac{\varepsilon_S-\varepsilon_\infty}{1+(i\omega\tau)^2}\right) - i\left(\frac{(\varepsilon_S-\varepsilon_\infty)\omega\tau}{1+(i\omega\tau)^2}\right) \qquad \text{Equation 1.10}$$

where the complex permittivity, $\varepsilon^*(\omega)$ is represented as function of the external oscillating electric field frequency, $f = \omega/2\pi$.

Figure 1.5 shows the typical shape of both ε′ and ε″ as function of the frequency in Hz. Relaxation can be detected as a peak in the imaginary part or as an inflexion in the curve of the real of the permittivity equation. The essential quantities which characterize a dielectric relaxation process can be extracted from that behaviour. The relaxation time of the fluctuation dipoles is given by $\tau = 1 / (2\pi \cdot f_{max})$, where f_{max} is the frequency at maximum ε″.[44]

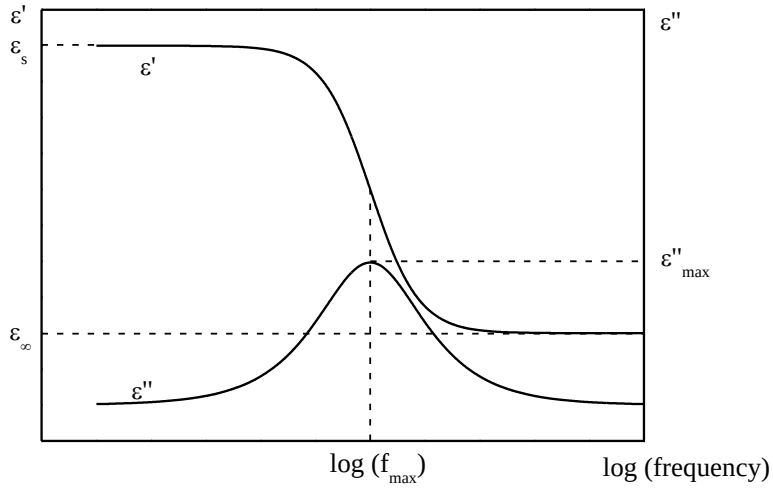

Figure 1.5- Frequency dependence of the real and imaginary permittivities in a simple Debye process.

Data analysis

To extract quantitative information from isothermal dielectric spectra as the relaxation time, dielectric strength, shape of the ε´´peak, it is necessary to adopt a mathematical expression to reproduce the experimental data. In this context, the empirical equation introduced by Havriliak-Negami is one of the more popular ones being applied successfully to several systems.[64, 65] In this work, this model function was fitted to both imaginary and real components of complex permittivity of each collected spectrum. Since, as above described, several relaxation processes can be detected originating multimodal peaks in the available frequency window, a sum of HN-functions should be is employed:

$$\varepsilon^*(f) = \varepsilon_0 + \sum_j \frac{\Delta\varepsilon_j}{[1+(i\omega\tau_{HN})^{\alpha_{HN}}]^{\beta_{HN}}} \qquad \text{Equation 1.11}$$

where j is the index over which the relaxation processes are summed, $\Delta\varepsilon$ is the dielectric strength, τ_{HN} is the characteristic HN relaxation time, and α_{HN} and β_{HN} are fractional parameters ($0< \alpha_{HN} \leq 1$ and $0< \alpha_{HN}\cdot\beta_{HN} \leq 1$) describing, respectively, the symmetric and asymmetric broadening of the complex dielectric function. Conductivity effects were taken into account at the beginning of crystallization by adding a contribution $\frac{\sigma_0}{\varepsilon_0\omega}$ to the imaginary part of the fit function where σ_0 is the d.c.-conductivity of the sample and ε_0 is the dielectric permittivity of vacuum.

From the estimated values of τ_{HN}, α_{HN} and β_{HN} fitting parameters, a model-independent relaxation time, $\tau_{max}= 1/(2\pi f_{max})$, can be determined according to the following equation:[66]

$$\tau_{max} = \tau_{HN} \times \left[sin\left(\frac{\alpha_{HN}\pi}{2+2\beta_{HN}}\right)\right]^{-1/\alpha_{HN}} \left[sin\left(\frac{\alpha_{HN}\beta_{HN}\pi}{2+2\beta_{HN}}\right)\right]^{1/\alpha_{HN}} \qquad \text{Equation 1.12}$$

Chapter II: Materials and Methods

This chapter present the materials and methods used in the different studies. Also, a synthesis and characterization of the confinement porous will be done, as well as a description of the impregnation method in the different host systems studied.

2.1 Triton X100

Triton X100, polyethylene glycol tert-octylphenyl ether, $C_{14}H_{22}O(C_2H_4O)_n$ (see Figure 2.1) with an average number, n ~9-10 of oxyethylene units per molecule (MW ~625) was reagent grade purchased from Fluka (catalogue number 93420; CAS number: 9002-93-1).

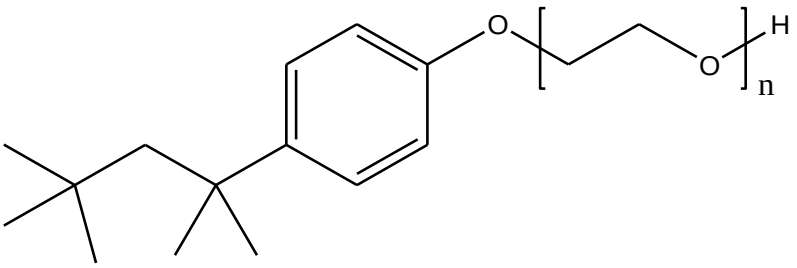

Figure 2.1 Chemical structure of Triton X100

A Karl Fisher analysis showed water content of 0.28% (w/w). It was used without further purification.

2.2 Confining porous host: Mesoporous silica based

2.2.1 SBA-15

The synthesis of the mesoporous silica based SBA-15 was carried out according to Gao et al. [67]The template using is a triblock copolymer, Pluronic P123. Typically, 2.0 g of triblock P123 was dissolved in 60 mL of 2 M aqueous HCl and 15 mL of distilled water under stirring. Then, when the solution was homogeneous and clear, 4.4 g of tetraethoxysilane (TEOS) (a silica source) was added dropwise to the solution at room temperature. The final mixture was stirred at 313 K for 24 h, transferred into a Teflon bottle sealed in an autoclave, and heated to 373 K for another 24h. Finally the resulting precipitate was filtered, washed carefully with distilled water, air-dried, and calcined at 773 K in air for 5 h to remove the template and to obtain the final product.

2.2.2 MCM-41

The preparation was carried out according to the literature.[68] The template, C_{18}TMABr, was dissolved in 120 g of deionized water to yield a 0.055 $mol \cdot l^{-1}$ solution, and 9.5 g of aqueous ammonia (25 wt.%, 0.14 mol) was added to the solution. While the surfactant solution was in stirred, 10 g of the TEOS

(0.05 mol) was added slowly. The resulting synthesis gel, having a molar composition of 1TEOS:0.152 C_{18}TMABr:2.8 NH3:141.2 H_2O , was stirred for one hour, then the white precipitate was filtered and washed with deionized water. After drying at 363 K for 12 h and to remove the template, the sample was calcined at 823 K (rate:1 $K \cdot min^{-1}$) for 5h in air.

2.2.3 Characterization of the mesoporous silica based

The nanostructured silica materials were characterized by X-Ray Diffraction (XRD), Nitrogen Adsorption and Tansmission Electron microscopy (TEM).

The mesoscopic structure was determinate by X-ray powder diffraction (XRD). Measurements were performed with a Miniflex – Rigaku/Bench-top X-ray Diffractometer (with Cu Kα radiation at 30 kV and 15 mA). For both of the porous materials, SBA-15 and MCM-14, X-ray diffraction pattern reveal the hexagonally structured pores (p6mm and p6m space group, respectively) at low angles, whereas no diffraction pattern can be observed at high angles due to the amorphous nature of the pore walls.

The porosity of the materials was characterized by Nitrogen adsorption/desorption isotherms and were measured at the liquid nitrogen temperature, using a 2010 V1.01B Micrometrics analyser. Samples were degassed at 373 K, under vacuum, for 24h before measurements. Specific surface areas were calculated using the BET method. Pore size distributions were evaluated from the adsorption branches of the nitrogen isotherms using the BJH method. The texture features obtained by nitrogen absorption analysis are presented in Table 2.1

Table 2.1. Properties of SBA-15 and MCM-41 samples.

Sample	BET Area [$m^2 \cdot g^{-1}$]	Pore diameter d [Å]	Pore volume Vp [$cm^3 \cdot g^{-1}$]
SBA-15	822	57.256	0.924
MCM-41	1106	34.175	1.030

Finally, to obtain structural information at nanometer scale resolution for porous materials, high-resolution TEM images were acquired with a Hitachi H8100/ThermoNoran System SIX (Electron Microscopy Laboratory, ICEMS/IST). Figure 2.2 shows transmission electron micrographs of representative regions of SBA-15 (a) and MCM-41 (b). Regular arrangement of the pores can be clearly observed for the both materials. These TEM images provide strong evidences that the support framework long range order was retained

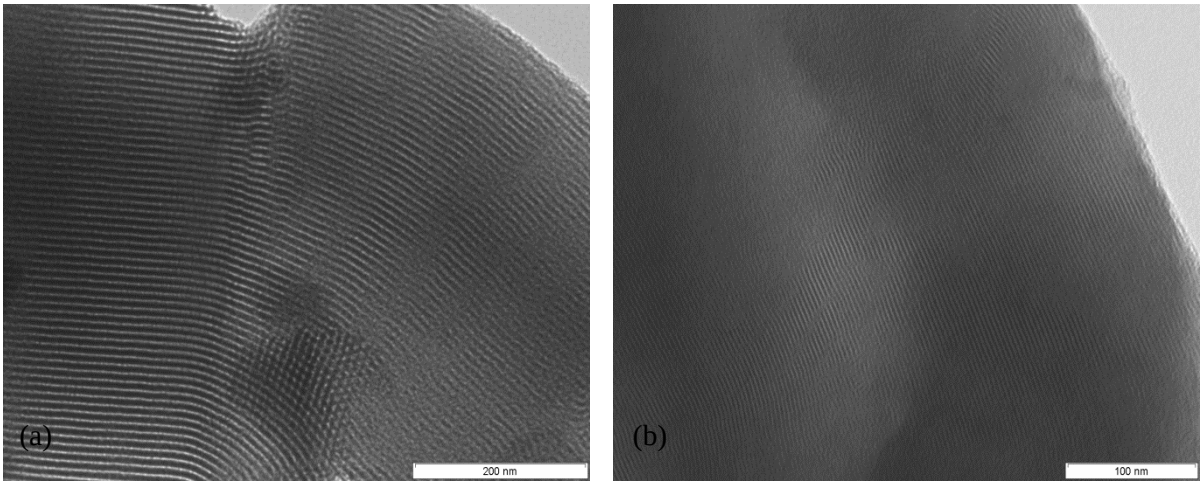

Figure 2.2. TEM pictures for the SBA-15 (a) and MCM-41 (b). The hexagonal ordering of the mesoporous materials is showing.

2.2.4 Experimental conditions: Impregnation protocol.

To remove water and other impurities adsorbed at the pore walls the matrix were evacuated under vacuum (10^{-4} mbar) at 393 K for 6 h.

A Triton X100 solution in ethanol was added to 0.1g of mesoporous silica based and kept 24 h under gentle stirring. Afterward, the suspensions were one night at room temperature and then, were washed with a small amount of ethanol to remove the excess of non-confined Triton X100. To remove the solvent, the samples were dried under vacuum at 358 K for 6 h. Then, the samples were stored in a desiccator.

The unloaded matrix, SBA-15, used to compared with the loaded matrix, was submitted to a protocol similar to the one used for impregnation using only ethanol.

The amount of Triton X100 with which the different solutions for impregnation were prepared, corresponds to twice the value estimated from the total pore volume for completely loading. This was done to ensure a high degree of filling.

2.3 Characterization techniques

2.3.1 Dielectric Relaxation Spectroscopy (DRS)

Dielectric measurements were carried out using the ALPHA-N impedance analyser from Novocontrol Technologies GmbH. A drop of Triton X100 was placed between two gold plated electrodes (diameter 10 mm) of a parallel plate capacitor, BDS 1200 with two silica spacers, 50 μm thickness. The sample cell was mounted on a cryostat, BDS 1100, and exposed to a heated gas stream being evaporated from a liquid nitrogen Dewar. The temperature control is assured by the Quatro Cryosystem and performed within ±0.5 K. Novocontrol Technologies GmbH supplied all these modules. Before the dielectric

measurements of bulk Triton X100, the sample was previously heated to 373 K, under the nitrogen stream, to eliminate residual water.

2.3.2 Differential Scanning Calorimetry (DSC)

The Triton X100 thermal characterization was carried out in Laboratorio de Análises (Departamento de Quimica da Universidadde Nova de Lisboa, FCT/UNL) by Differential Scanning Calorimetry (DSC) using a DSC 131 model Setaram Calorimeter. Samples of 20 mg were weighed in 100 µl aluminium pans (6 mm base diameter, 4.2 mm deep). An empty pan was used as reference. An indium sample was used as calibration standard for both temperature and heat flow (m.p. 429.7 K, heat of melting 3263.5 $J \cdot mol^{-1}$). Measurements were carried out under a nitrogen atmosphere with a flow rate around 20 $ml \cdot min^{-1}$.

The samples were submitted to a first heating for 5 min at 373 K in order to eliminate the water residues.

For the confined materials the DSC experiments were carried out in a DSC Q10 from TA Instruments with a cooling/heating rate of 20 $K \cdot min^{-1}$ covering the temperature range from 143 K to 373 K (the high heating rate was used in order to increase the intensity of the heat jump capacity associated to the glass transition of Triton X100 confined to SBA-15 mesopores). A small amount of sample (less than 5 mg) was placed in an open aluminum pan. Measurements were realized under dry helium (at flow rate of 25 $ml \cdot min^{-1}$) to improve the thermal conductivity. A liquid nitrogen cooling system was used in order to reach temperatures as low as 143 K. Temperatures and enthalpies were calibrated using Indium at the same heating rate and the same environmental conditions as the experiments.

These measurements were carried out in the laboratory UMET from University of Lille 1.

2.3.3 Polarized Optical Microscopy (POM)

Polarized Optical Microscopy was performed on a Olympus Bx51 optical microscope equipped with a Linkam LTS360 liquid nitrogen-cooled cryostage. The microstructure of the sample was monitored by taking photomicrographs at appropriate temperatures and intervals of time, using an Olympus C5060 wide zoom camera. Images were obtained at a magnification of 500x. A drop of Triton X100 was squeezed between two microscope slides and inserted in the hot stage. The thickness of the squeezed sample was ca. 50 µm. Before each measurement the Triton X100 sample was heated up to 373 K and kept 5 minutes at this temperature to allow complete melting.

2.3.4 Thermo Gravimetric Analysis (TGA)

The thermo-gravimetric measurements were carried out with a TGA 7 apparatus from Perkin-Elmer under highly pure nitrogen atmosphere with a flow rate of 20 $ml \cdot min^{-1}$. The temperature reading was calibrated using the Curie points of alumel and nickel standards, while the mass reading was calibrated using balance tare weights provided by Perkin-Elmer.

In this work, the weight loss due to the burning and decomposition of the organic molecules is measured up to ca. 800 K while the SBA-15 matrices are thermally stable up to temperatures above 1000 K (its weight is constant by increasing the temperature up to 1073 K).

TGA measurements were carried out in the laboratory UMET from University of Lille 1. The author acknowledges Madame Florence Danède

2.3.5 ATR-FTIR

Fourier Transform Infrared (FTIR) spectra over the range from 350 to 4000 cm^{-1} were collected at room temperature (~ 272 K) using Nicolet Nexus 670 FT-IR spectrometer equipped with a Germanium attenuated total reflection (ATR) accessory, a DTGS KBr detector and KBr beam splitter. All the spectra were taken via the ATR method, in the wave number range from 350 to 4000 cm^{-1} with a resolution of 2 cm^{-1} using 60 scans. FTIR measurements were carried out in the laboratory LASIR from University of Lille 1. The author acknowledges Prof. Nacer Idrissi.

Chapter III: Results and Discussion

In the first part of this chapter, the phase transformations of the surfactant Triton X100 were investigated using DSC and DRS.

Due to its high dielectric response and ability to crystallize from both molten (melt-crystallization) and glassy (cold-crystallization) states, Triton X100 is a good candidate to study simultaneously the crystallization process and the mobility of the coexistent amorphous fraction. In particular, the differences in molecular mobility, investigated by DRS, of the remaining amorphous fraction upon both isothermal and nonisothermal crystallization are evaluated, allowing inferring about the achieved semicrystalline morphology.

The isothermal cold and melt crystallization were monitored near above the calorimetric glass transition temperature by POM (221 K) and real-time DRS (T_{cr} = 219, 220 and 221 K) to evaluate the phase transformation from an amorphous to a semi-crystalline material.

This study was preceded by the investigation of the completely amorphous Triton X100.

Some of the results presented in this chapter have already been published. [69]

3.1 Characterization of the amorphous state

To obtain Triton X100 in amorphous state at temperatures below the melting point, the sample was first heated up to 373 K to assure water removal and then cooled down to 153 K at the maximum cooling rate reached by the DRS equipment (≈11 K·min^{-1}) (see figure 3.1).

To confirm that no crystallization occurred, the increase observed in ε´ trace (see arrow in the figure) will be taken now for analysis. This rise in the dielectric permittivity is related to the expected increase of the dielectric strength which can be quantified according to Fröhlich-Kirkwood equation: [66, 70]

$$\boldsymbol{\varepsilon_S - \varepsilon_\infty = \frac{\mu_0^2 g N/V \varepsilon_s (\varepsilon_\infty + 2)^2}{9\varepsilon_0 k_B T (2\varepsilon_S + \varepsilon_\infty)}} \qquad \text{Equation 3.1}$$

where μ_0 is the dipolar moment of the isolated dipole, g takes into account the dipole-dipole correlation (for parallel or anti-parallel correlations between neighbouring dipoles, g>1 or 0<g<1, respectively, while for a random orientation distribution of dipoles, g = 1), ε_S and ε_∞ are the limits of the real part of the dielectric permittivity at low and high frequencies respectively, the latter being approximately the permittivity of the glass,[71] ε_0 is the vacuum permittivity, N/V is the number of dipoles per unit of volume and k_B is the Boltzmann constant. Thus, from equation 3.1 the dielectric strength ($\Delta\varepsilon = \varepsilon_S - \varepsilon_\infty$) is proportional to $\mu_0^2 g / 9\varepsilon_0 \, k_B T$. If it is assumed that g is constant, an increase in

Δε from 375.4 K to 249.6 K of 33.5% is predicted. The observed raise is 34.9 % ($\varepsilon'_{375.4\ K}$ = 6.73;

$\varepsilon'_{249.6\ K}$ = 9.08) confirming that no dipolar moment is lost due to immobilization that would occur if crystallization had taken place. This was confirmed later by DSC. The circumvention of crystallization allowed obtaining Triton X100 as a supercooled liquid that becomes a glass upon further cooling, and so it is classified as a glass former.

Therefore to evaluate the mobility in the thus obtained glass and supercooled liquid state, dielectric loss spectra were taken at different increasing temperatures steps from 153 K up to 273 K: in the temperature range 153 K ≤ T ≤ 193 K and 273 K ≤ T ≤ 373 K each spectra was recorded every 5 K; in the remaining temperature region the spectra were recorded every 2 K.

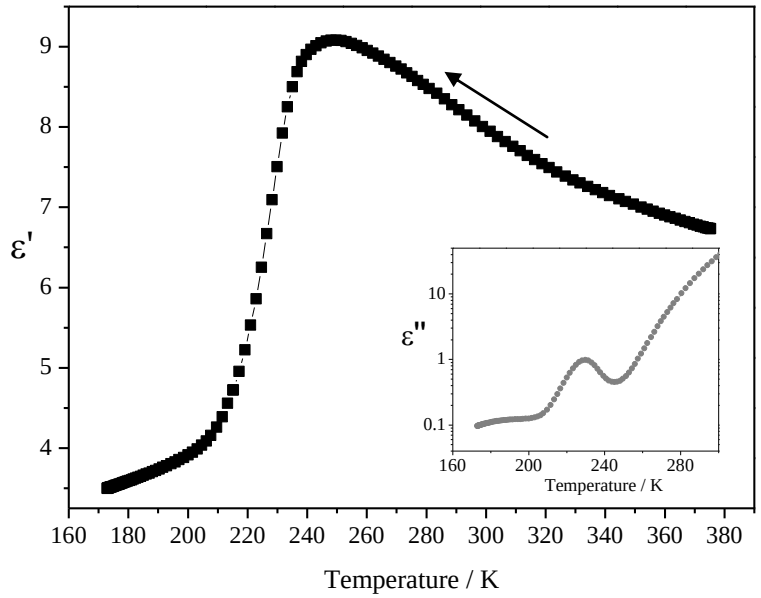

Figure 3.1 Isochronal plot of the real permittivity, ε´, at 10 kHz during the cooling process is show; the respective imaginary part, ε´´ is presented in the inset. The absence of discontinuity in both traces ε´and ε´´ upon cooling, conclude that the crystallization is avoided when the Triton X100 is cooling down at a rate of $\approx 11\ K \cdot min^{-1}$.

The values of ε" collected isothermally between 153 and 223 K are shown in figure 3.2.The spectra evidence a multimodal character with several relaxation processes; this was also evident in the ε´´ trace shown previously in the inset of figure 3.1. At the lowest frequencies a strong relaxation process is observed, which will be attributed later on to the dynamic glass transition; therefore it is designated hereafter as α-process. This process shifts to higher frequencies with the temperature increase, which is an expected observation due to the mobility enhancement provide by the temperature increasing. At the lowest temperatures, a weaker but well defined process is found that also goes towards high frequencies with T increasing, although in a less extent. In between both processes another one is felt but never emerging as a definite one. With the temperature increase, crystallization occurred between 221 and 223 K, as confirmed by the abrupt decrease in the spectrum taken at the latter temperature (seen the isotherms in the inset in figure 3.2).

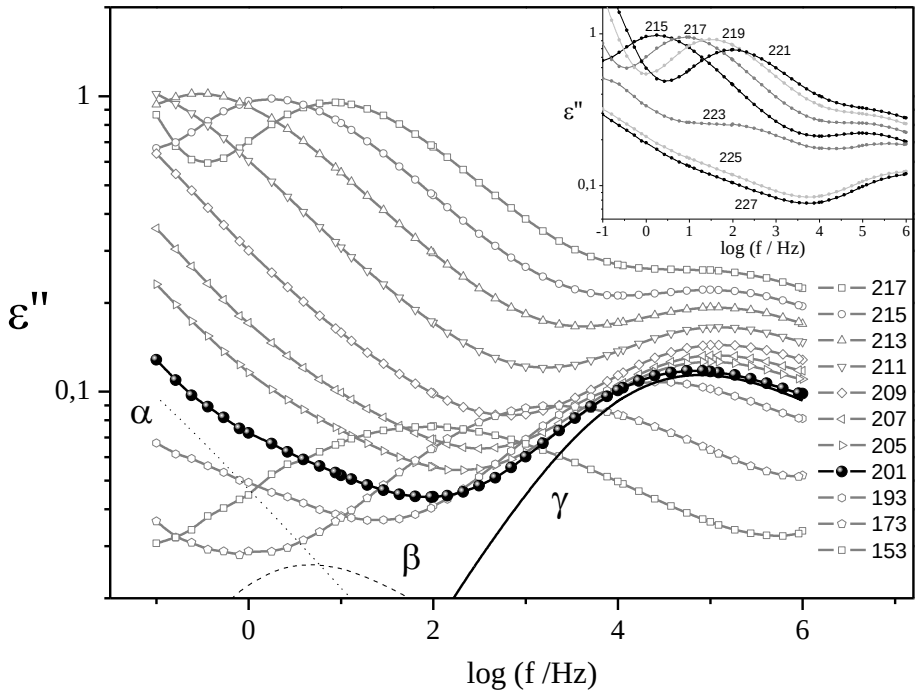

Figure 3.2 Isothermal dielectric loss spectra between 153 K and 217 K, after a cooling ramp carried out at 11 $K \cdot min^{-1}$ from 298 K to 153 K are illustrated. To ilustrate the two secondary processes detected at low temperatures, the overall HN fit to the experimental data for 201 K is show; the corresponding HN individual curves are also included. In the inset, the isothermal dielectric loss spectra taken during the crystallization are show.

To evaluate the temperature dependence of the relaxation times of each detected process in the amorphous state before crystallization, equation 1.11 (HN) was fitted to each spectrum allowing drawing a relaxation map (figure 3.3) (the empirical HN function was described in the Introduction).

The relaxation processes were designated as usual in an increasing order of frequency at which they are detected for a fixed T, as α, β and γ. The temperature dependence of the relaxation times of the γ-process is Arrhenian as characteristic of a localized relaxation process (see *Introduction* section 1.2) confirming that it is thermal activated. Although not so well defined also a linear plot is obtained for the β-process, while the usual VFT curvature is obtained for the α-process denoting the cooperative nature of the underlying relaxation mechanism.

The solid line for this α-process is the fit obtained from the VFT law to the τ(T) data (equation 1.1). From the extrapolation of the VFT equation to τ = 100s a glass transition temperature of 209.1 K is obtained; the respective VFT parameters are given in table 3.1.

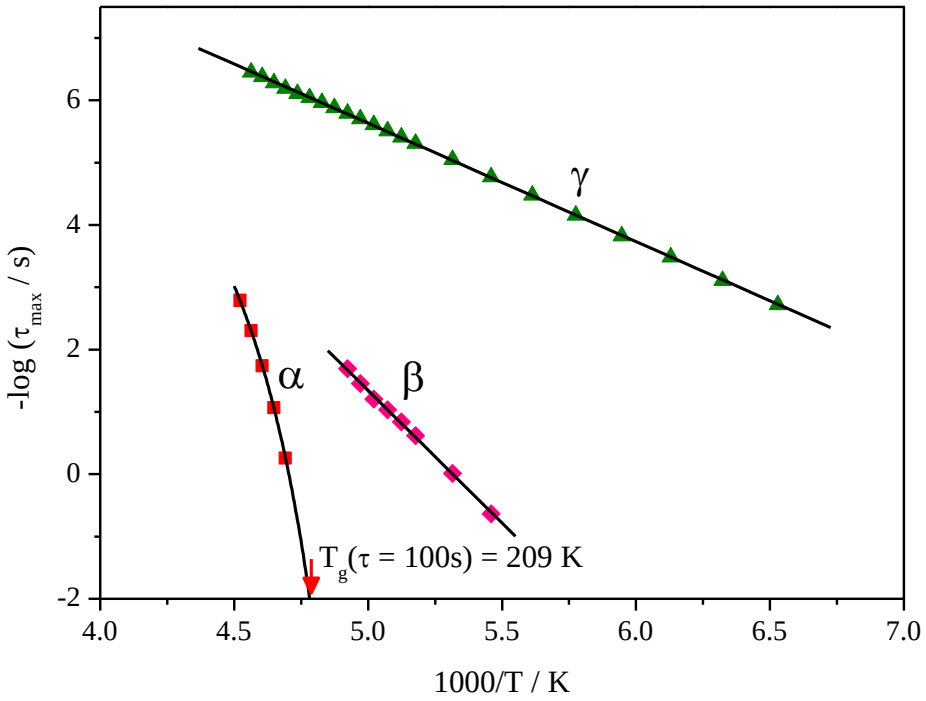

Figure 3.3 Relaxation time, τ, versus 1/T for all processes obtain from the isothermal loss data collected during heating. Lines are fits of the Arrhenius and VFTH formulas to the corresponding data. The arrow indicates the location of the estimate T_g at 100s.

The summary of all activation parameters for the three processes is presented in table 3.1.

Table 3.1. Parameters obtained from Arrhenius and VFT fitting for the relaxations detected for the amorphous Triton X100.

Secondary process :Arrhenius parameters			**α-process: VFTH parameters**	
	γ-process	β-process	α-process	
E_a / kJ·mol-1	36.4 ± 0.1	81.5 ± 1.1	**$E_a(T_g)$ / kJ·mol^{-1}**	590.8 ± 67
τ_∞ / s	(7.5 ± 4.7) x 10^{-16}	(2.3 ± 1.6) x 10^{-23}	**τ_∞/ s**	(1.1 ± 0.2) x 10^{-09}
			T_0 / K	193.6 ± 0.2
			T_g (τ=100s) / K	209.1 ± 0.6
			B / K	392.8 ± 7.3

It is interesting to note that in spite of the depletion of the cooperative α-process, the localized β and γ processes persist even after crystallization. In the next section the influence of thermal history in the Triton X100 transitions, including crystallization will be evaluated.

3.2 Study of the Thermal Transitions of the Triton X100

3.2.1 Experimental conditions

3.2.1.1 Differential Scanning Calorimetry (DSC)

The thermal properties of the Triton X100 were investigated by DSC. The samples were submitted to a first heating for 5 min at 373 K in order to eliminate the water residues.

The influence of cooling rate in the thermal properties of Triton X100 was evaluated carrying out different cooling/heating cycles between 373 and 143 K with cooling rates of 13 $K \cdot min^{-1}$ (cycle I), 9 $K \cdot min^{-1}$ (cycle II), 5 $K \cdot min^{-1}$ (cycle III), 1 $K \cdot min^{-1}$ (cycle IV) and 0.5 $K \cdot min^{-1}$ (cycle V), the subsequent heating scans were carried out from 143 to 373 K always at a heating rate of 10 $K \cdot min^{-1}$.

The reversibility of the thermal transitions was verified by reheating the cooled sample just after the preceding scan up to its transition temperature.

3.2.1.2 Dielectric Relaxation Spectroscopy (DRS)

Before all dielectric measurements, the Triton X100 sample was previously heated to 373 K during 10 minutes, under the nitrogen stream, to eliminate residual water.

In order to study the thermal transitions of Triton X100, isochronal measurements of the complex permittivity were carried out at 10^2 Hz, 10^3 Hz, 10^4 Hz, 10^5 Hz and 1 MHz, during cooling/heating cycles with different cooling rates and the subsequent heating performed always at 9 $K.min^{-1}$. The actual cooling rates were 11 $K \cdot min^{-1}$ (cycle 1), 7 $K \cdot min^{-1}$ (cycle 2), 4 $K \cdot min^{-1}$ (cycle 3), 1 $K \cdot min^{-1}$ (cycle 4) and 0.5 $K \cdot min^{-1}$ (cycle 5).

3.2.2 Calorimetric studies.

The thermal behaviour of Triton X100 was investigated in the temperature range between 143 and 373 K. It was observed that it crystallizes or vitrifies upon cooling from the equilibrium liquid depending on the cooling rate.

Figure 3.4 presents the DSC thermograms collected on cooling at two representative rates a) 9 $K.min^{-1}$ and b) 1 $K \cdot min^{-1}$ and the subsequent heating run recorded at 10 $K \cdot min^{-1}$. For the thermogram collected at the highest cooling rate no transition occurs down to ~210 K, temperature at which the heat flux presents a discontinuity characteristic of the glass transition; the same is true for the thermogram collected on cooling at 13 $K.min^{-1}$ (not shown). Therefore at these highest rates it was possible to circumvent crystallization as already achieved by DRS confirming that Triton X100 is a glass former Microphotographs taken by POM (see *Materials and Methods* section 2.3.3) on cooling from 373 K down to 193 K at 10 $K.min^{-1}$ show an isotropic structure in the liquid state that remains in the supercooled region and glassy state (see figure 3.4 a -cooling).

By other side, the thermogram collected at 1 K.min^{-1} shows an exothermal peak centred at around 255 K (see table 3.2). This is due to spherulitic crystallization confirmed by POM (see microphotograph in figure 3.4 b - cooling).

Melt crystallization is also observed during cooling at 5 and 0.5 K·min^{-1} (not shown), with a temperature onset that increases with the cooling rate decrease.

Concerning the subsequent heating runs presented in figure 3.4 a), for the one collected after cooling at 9 K.min^{-1}, the heat flow jump reappears taken as the glass transition signature at a temperature of 212 K taken at the midpoint of the transition region (data provided in table 3.2); this value of the glass transition temperature agrees with the values provided for Triton X100 by Jensen *et al* [72] (214.5 K measured at the midpoint) and by Larraz *et al* [73] (205.15 K measured at the onset). Moreover, it is in good accordance with the value (209 K) estimated from DRS.

Table 3.2Thermal properties of Triton X100 obtained by DSC during different cooling/heating cycles: T_g – glass transition temperature determined at the inflection point; T_m- melting temperature corresponding to the endothermic peak of the melting transition; T_{cr}- crystallization temperature corresponding to the exothermic peak of the crystallization transition; ΔH_m and ΔH_{cr} – melting and crystallization enthalpies, respectively

Cycle	Cooling scan				Heating scan at 10 K·min^{-1}				
	Rate (K·min^{-1})	Glass transition	Melt crystallization		Glass transition	Cold crystallization		Melting	
		T_g/ K	T_{cr}/ K	ΔH_{cr}/J·g^{-1}	T_g/ K	T_{cr}/ K	ΔH_{cr}/J·g^{-1}	T_m/ K	ΔH_m/J·g^{-1}
I	13	206.7	no	no	212.2	232.2	-65.6	277.2	62.5
II	9	206.5	no	no	211.9	232.1	-64.8	277.2	61.6
III	5	208.0	227.3 248.5	-1.4 -0.8	212.0	231.5	-60.7	277.2	61.4
IV	1	*	254.7	-71.9	214.1	n.o.	n.o.	273.2	72.0
V	0.5	*	260.3	-81.4	data not available				

* it is not possible to give an accurate value

At higher temperatures, at 232 K, a sharp exothermic peak characteristic of cold crystallization emerges followed by a broad endothermic peak with minimum at 277 K, due to melting; details on temperatures and enthalpies are provided in table 3.2. Cold-crystallization in the sample previously cooled at 10 K·min^{-1} was also observed by POM by the appearance of a grain-like structure (microphotograph in figure 3.4 a-heating). This crystalline structure slowly melts finally disappearing at around 273 K in accordance with the broad melting endotherm observed by DSC.

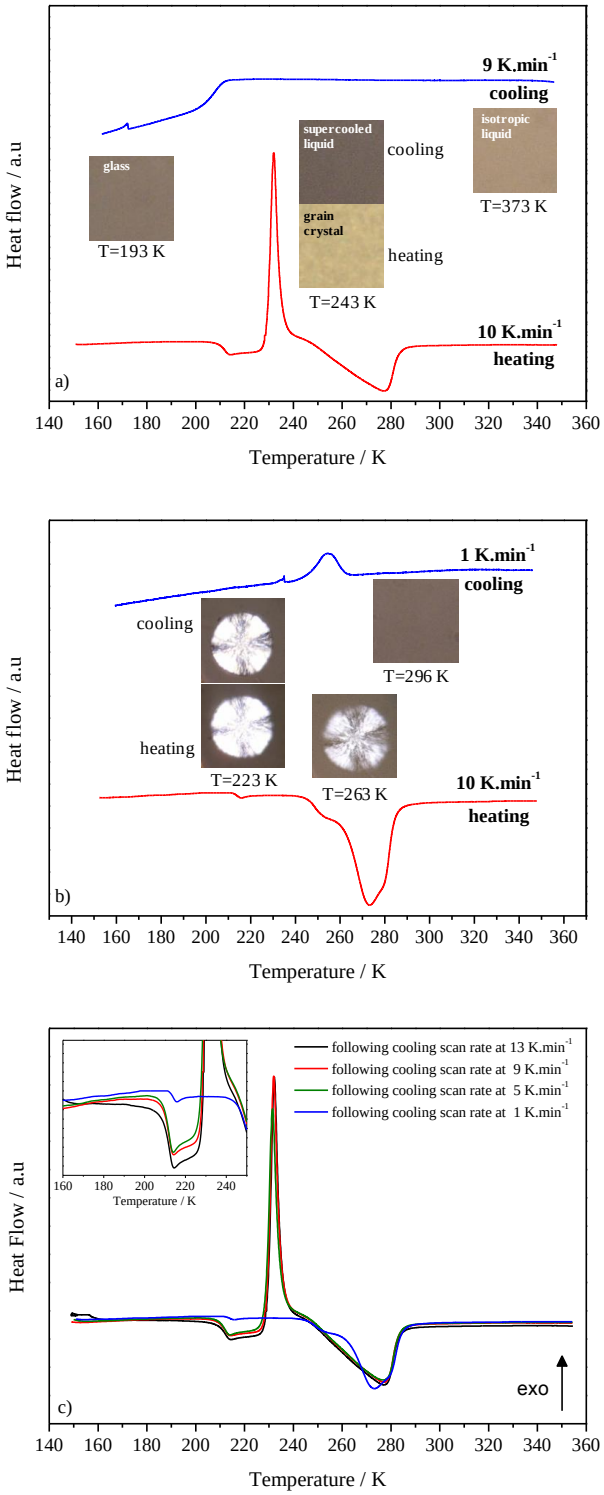

Figure 3.4 Thermograms (heat flow in arbitrary units, a.u., vs. temperature) of Triton X100 after water removal at 373 K collected at two cooling rates, a) 9 K·min^{-1} and b) 1 K·min-^{1}, and subsequent heating scans at 10K·min^{-1} as measured by differential scanning calorimetry; different heat flow scales were used for heating and cooling. c) Heating scans collected at 10 K·min^{-1} after all tested cooling rates; the inset is a scale up of the glass transition region evidencing that the heat flux jump occurs in all heating scans. Microphotographs taken by POM at the specified temperatures on cooling from the liquid state at 10 K·min^{-1} and on heating from the glass at 5 K·min^{-1} are included in Figures a) and b).

With the exception of the heating run taken after cooling at 1 $K \cdot min^{-1}$, all the runs present the sharp exotherm due to cold-crystallization and posterior endotherm owing to melting (figura 3.4 c). In fact, in the heating run measured after cooling at 1 $K \cdot min^{-1}$, no crystallization is observed, the main thermal event being an endotherm centered at 273 K corresponding to the melting of the crystalline fraction previously formed. The microphotograph taken by POM (figura 3.4 b-heating) evidences the partial melting of the spherulite that exhibits a weaker intense birefringence pattern compared with the original one; once again the melting occurs gradually as observed also by DSC. The absolute values of the enthalpies determined by DSC of previous crystallization and subsequent melting on heating, are equal (72 $J \cdot g^{-1}$) confirming that the material in this condition didn't undergo further cold crystallization. Moreover, the detection of the glass transition (scale up in the inset of figure 3.4 c) reveals that the material although having crystallizing in a great extent as denoted by the high value of the crystallization enthalpy as compared to the other runs, is in the semi-crystalline state. The glass transition step was detected in all cases, as evidenced in inset, revealing that indeed in all runs a semi-crystalline material was obtained.

3.2.3 Dielectric Relaxation Spectroscopy

3.2.3.1 Thermal transitions probed in isochronal mode.

The influence of cooling rate was also evaluated by DRS. Figure 3.5 presents the isochronal plots of both ε´ and ε´´ (in inset) at 10 kHz collected in the descending run to 160 K at the highest cooling rate (11 $K \cdot min^{-1}$). The corresponding heating run performed at 9 $K \cdot min^{-1}$ is represented in black symbols.

The trace of the real part, ε´, of the complex permittivity during cooling reproduces the plot obtained earlier before the collection of isotherms to investigate the amorphous state. It shows the initial rise with the temperature decrease, followed by a marked fall indicating the transformation, at the measuring frequency, from the supercooled liquid to the glass; in the ε´´ trace, this corresponds to an intense peak i.e. the α-relaxation process associated to the dynamical glass transition, already investigated for the amorphous state in the previous section. At the lowest temperatures, a broad and low intense peak is observed due to the secondary β and γ relaxations previously detected.

Upon the subsequent heating, the fully amorphous sample undergoes cold-crystallization,[74, 75] which is visible in the plot just above 230 K by an abrupt decrease in both ε´and ε´´as found also previously. The further increase in both real and imaginary parts observed near above 240 K is due to the progressive melting of the crystalline fraction thus formed; the ε´ and ε´´ values superimpose those of the equilibrium liquid at a temperature around 280 K which is a frequency independent thermal event. Both temperatures are in a very good agreement with the onset and midpoint of the melting endothermic peak detected in the correspondent DSC heating thermogram, respectively, 243 K ($T_{m,\,on}$) and 277 K ($T_{m,\,peak}$).

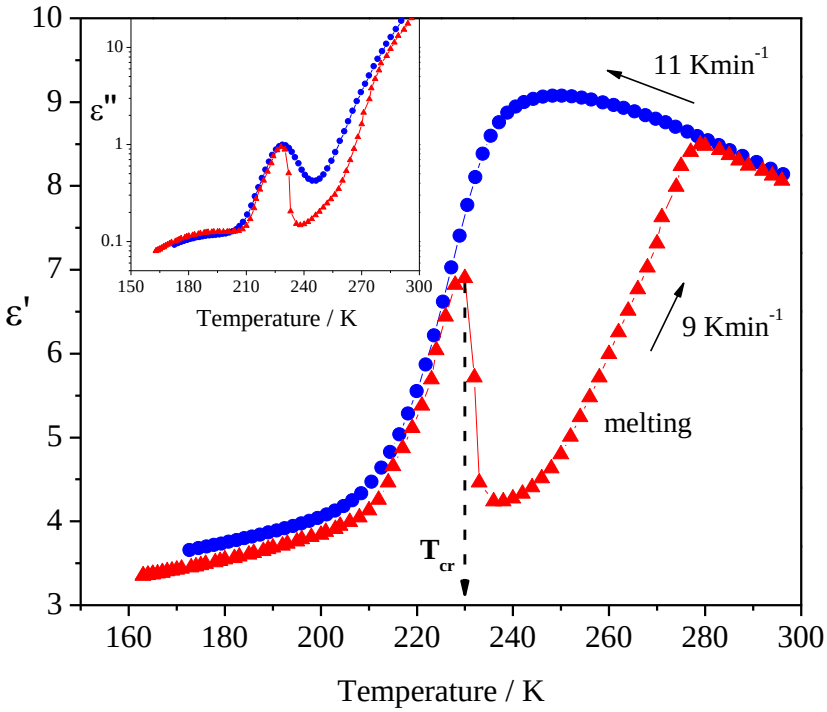

Figure 3.5 Isochronal plots of the real, ε´, and imaginary, ε´´ (inset) parts of the complex permittivity at 10 kHz collected in a cooling ramp from 298 to 160 K (circles) and the subsequent heating ramp (triangles) carried at the specified rates; while crystallization was circumvented during cooling, the drop in both ε´and ε´´ traces reveals that it occurred upon heating.

Figure 3.6 shows the isochronal plots of ε´ traces collected upon a) cooling at different rates and b) subsequent heating at 9 K·min^{-1}.

The ε´ trace obtained at a cooling rate of 11 K·min^{-1} (figure 3.6 a) acts as a reference for a run in which the sample does not undergo crystallization from the melt. Therefore, it was concluded that the sample undergoes crystallization in all runs except the one taken at the highest cooling rate. Moreover, the temperature at which crystallization occurs increases with the decrease of cooling rate. These observations are coherent with the previous reported DSC results.

In the following heating run, cold-crystallization is observed, as already mentioned from the drop in the ε´ trace when the sample was previously cooled at 11 K·min^{-1} and by the decrease in the ε´´ peak as well as shown in the inset (Figure 3.6 b). In general, the ε´´-peak associated with the dynamic glass transition observed on the heating run, emerges smaller with the decrease of the cooling rate of the preceding run. A more detailed analysis reveals that in the heating run after cycle 3 no further cold-crystallization occurs: no drop in either ε´ or ε´´ traces is observed. This could lead us to conclude that the sample is fully crystalline. However, it stills in the semi-crystalline state since a relaxational

contribution associated with the glass transition exists (see the respective ε´´-peak in the inset in figure 3.6 b), although significantly depleted.

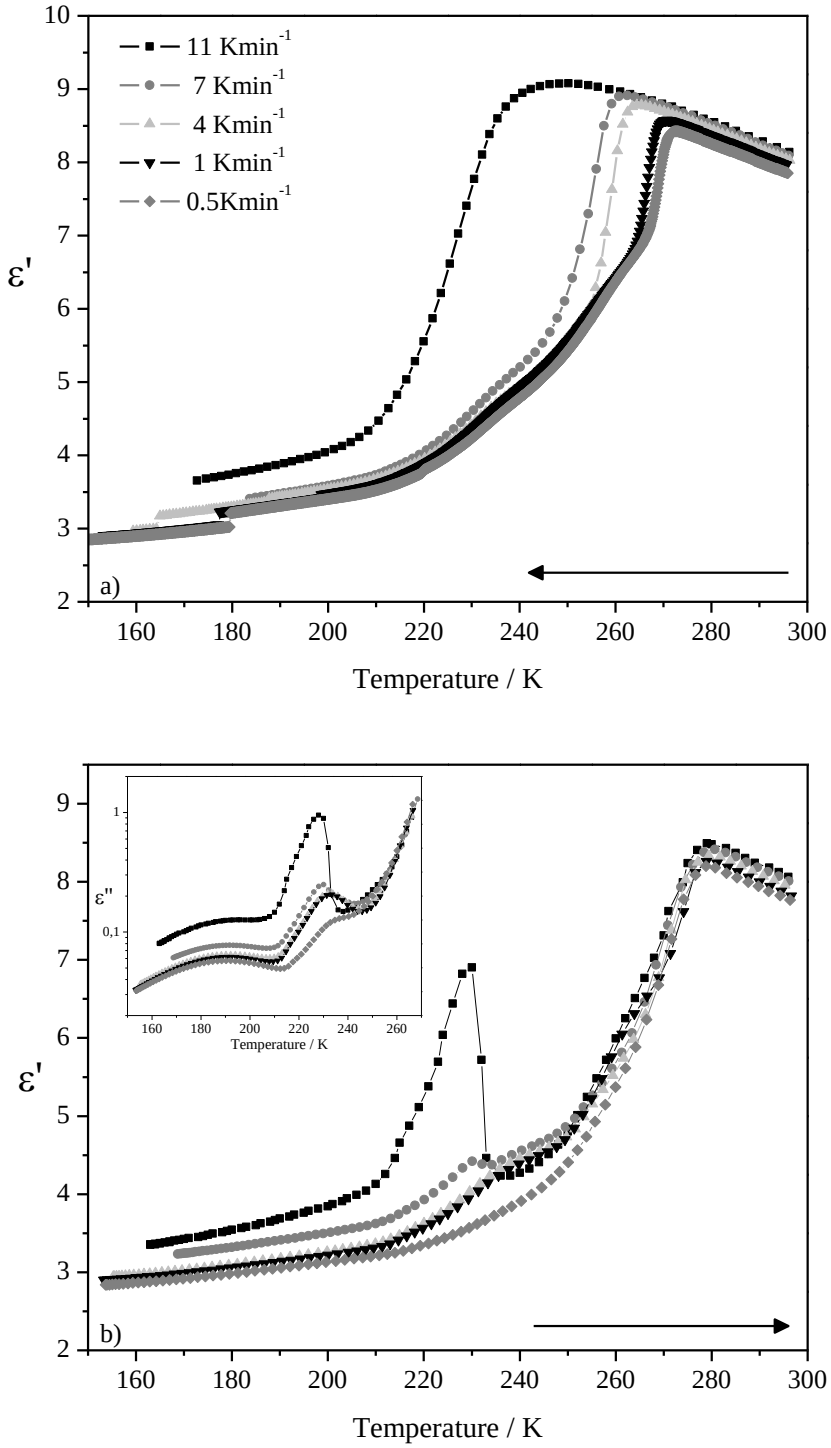

Figure 3.6 Isochronal plots of the real permittivity, ε´, at 10 kHz during a) cooling ramp experiments carried at different rates (see legend) and b) during the heating run, followed immediately after the cooling, which was performed always at the same rate (9 $K \cdot min^{-1}$) (same colours and symbols apply). The inset presents the corresponding isochronal loss trace, ε´´, obtained during heating evidencing the depletion in the α-process due to crystallization.

For all runs the endset of the melting is detected at the same temperature, close to 280 K, as observed in DSC.

Ramp experiments carried out at different cooling rates by either DSC or DRS proved that the glass-former Triton-X can be obtained with different extents of crystallinity, the slower rates promoting a higher crystallization, as expected.

DRS measurements evidence that a fully amorphous material is obtained when cooling from the liquid state at cooling rates higher than 10 $K \cdot min^{-1}$. On the other hand, a fully crystalline material could not be obtained by slow cooling experiments neither by DRS nor DSC.

3.2.3.2 Real time dielectric measurements during isothermal crystallization

To get a further insight in the crystallization behaviour, isothermal crystallization from both glassy and molten states was promoted and monitored in real-time by dielectric relaxation spectroscopy at 219, 220 and 221 K (see *Materials and Methods* section 3.2.1). These temperatures were chosen since allow simultaneously the detection of the α-process within the experimental frequency window and the amorphous-crystalline inter-conversion in a reasonable time. Figure 3.7 shows the collected loss spectra for cold-crystallization at some representative times. It must be noted that the same profile was obtained during real time measurements for melt-crystallization at the same temperature, at each T_{cr}, being the reason why it is not shown here. The main observation is the strong depletion of the α-process. At the high frequency flank of the dominant process, the secondary relaxation is detected; an additional process is also felt at the lowest frequencies. Whether this process is a MWS one or an α'-process as found in crystallizable systems either polymeric [14, 29, 76] or low molecular weight materials,[4, 21] or even the simultaneous contribution of a secondary process which is merged under the main alpha process in the fully amorphous material or a low frequency one, it is not clear up to now. This process should not be confused with conductivity, since the latter only affects the spectra at the first crystallization times. This is demonstrated by carrying out the analysis proposed by Dias [77], an alternative to the numerical Kramers–Kronig transform, based on the logarithmic derivative of the real permittivity given by $\varepsilon''_{der} = -\pi/2(\partial\varepsilon'(\omega)/\partial \ln\omega)$ that allows to eliminate the conductivity contribution from ε´´. In figure 3.7 for T_{cr}=219 K , ε''_{der} is plotted at some definite crystallization times (thicker solid lines) where is obvious the coincidence between the experimental and the estimated ε´´for longer crystallization times reinforcing that the low frequency contribution is other than conductivity. Therefore a sum of 3 processes was considered in the HN fit to the experimental ε´and ε´´ data (equation 1.11). The parameters of the individual functions used to fit the complex permittivity spectra for each temperature and type of crystallization are summarized in table 3.4; since the peak of the low frequency process never shows up at any of the tested crystallization temperatures, no fitting parameters will be provided here. It was found that for all tested crystallization temperatures both real

and imaginary parts of the complex permittivity spectra are perfectly fitted by maintaining fixed both α_{HN} and β_{HN} shape parameters and τ_{HN} of the main process; the overall fit to ε'' is presented in figure 3.7 as solid lines. Therefore, the α-relaxation keeps both shape and location invariants during isothermal crystallization (either cold or melt). The secondary relaxation also keeps the same shape; the respective relaxation times were allowed to vary, but no significant shift was observed (see limits in table 3.3).

Table 3.3 HN parameters (α_{HN}, β_{HN}, τ_{HN}) fixed in the fitting procedure to the complex permittivity spectra during isothermal cold and melt crystallization; τ_{max} is the model-independent relaxation time obtained from τ_{HN} (equation 1.12).

	α-relaxation					Secondary relaxation		
	T_{cr} /K	α_{HN}	β_{HN}	τ_{HN} / s	τ_{max} / s	α_{HN}	β_{HN}	τ_{HN}/s [a)]
Cold-crystallization	219	0.58	0.57	1.35×10^{-2}	5.49×10^{-3}	0.50	0.36	t_{0s} 2.5×10^{-6} → t_{8640s} 1.3×10^{-6}
	220	0.58	0.57	6.25×10^{-3}	2.51×10^{-3}	0.49	0.36	t_{0s} 1.7×10^{-6} → t_{7560s} 1.2×10^{-6}
	221	0.59	0.57	3.09×10^{-3}	1.28×10^{-3}	0.56	0.36	t_{0s} 1.6×10^{-6} → t_{4500s} 1.1×10^{-6}
Melt-crystallization	219	0.60	0.57	1.34×10^{-2}	5.64×10^{-3}	0.45	0.36	t_{0s} 2.9×10^{-6} → t_{8640s} 1.4×10^{-6}
	220	0.55	0.56	6.0×10^{-3}	2.4×10^{-3}	0.42	0.36	t_{0s} 1.8×10^{-6} → t_{7560s} 1.4×10^{-6}
	221	0.58	0.57	3.5×10^{-3}	1.42×10^{-3}	0.51	0.36	t_{0s} 2.7×10^{-6} → t_{4500s} 1.6×10^{-6}

a)The τ_{HN} values varied between the given limits during crystallization.

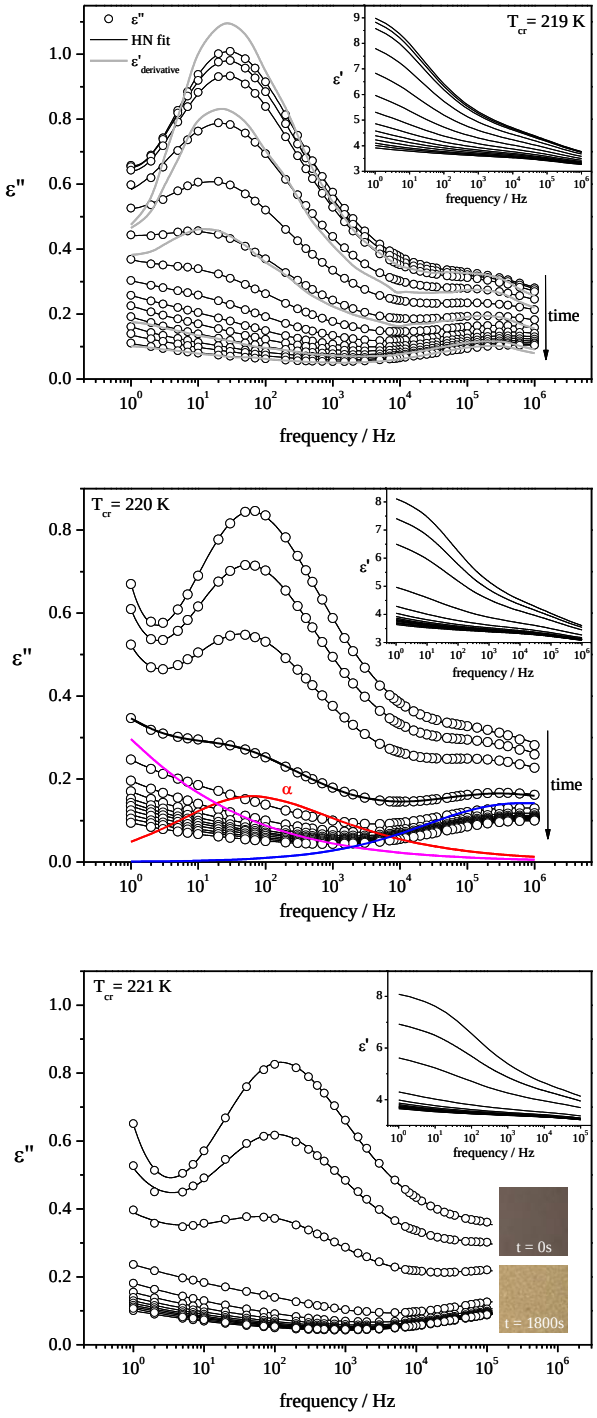

Figure 3.7 Real time evolution of imaginary part of the complex permittivity, ε´´(f), during isothermal cold crystallization: only some representative loss spectra are illustrated- the two first spectra being 180 s apart and the following being 360 s apart. The α-process dominates the spectra and the secondary relaxation influences the spectra in the high frequency side while a low frequency process is needed to adequately simulate the loss data. Solid lines are the overall fit where a sum of 3 HN individual processes was considered (see text); these 3 HN processes are exemplified for T_{cr} = 220 K for the spectrum taken at 720 seconds (thicker solid line). For T_{cr} = 219 K the logarithmic derivative of the real permittivity is represented for some crystallization times as gray thicker solid lines, allowing to eliminate the conductivity contribution from ε´´. For T_{cr} = 221 K, POM microphotographs taken at the initial time and after 1800 s were included; a scale-up of the grainy morphology observed at t_{cr}=1800 s is shown later on Figure 3.10. The inset in the Figures represents the evolution of the respective real part ε´(f).

From the HN fit the dielectric strength, Δε, is also obtained (see equation 1.11). Its time evolution during both cold and melt crystallization for each T_{cr} is shown in figure 3.8.

The variation with the crystallization time of the dielectric strength reduced by the initial value, can be used to estimate the crystallinity degree (χ_{cr}), considering that the relaxation intensity is proportional to the amount of non-crystalline phase.[71] When crystallization leads to the extinction of the main α-process and no significant dielectric response persists in the detected processes observed in the frequency window which is being probed, it is common to consider χ_{cr} as 1 - ($\Delta\varepsilon_{\alpha,t}/\Delta\varepsilon_{\alpha,0}$).[4, 5, 78] However, it is clear from both, figure 3.7 and figure 3.8, that the secondary process is still active after the vanishing of the α-relaxation. Therefore, the simultaneous contribution of both processes will be taken in account to quantify the degree of crystallinity according to:

$$\chi_{cr}(t) = 1 - \frac{\Delta\varepsilon_{\alpha}(t)+\Delta\varepsilon_{\gamma}(t)}{\Delta\varepsilon_{\alpha}(t=0)+\Delta\varepsilon_{\gamma}(t=0)} \qquad \text{Equation 3.2}$$

The time dependence of the crystallinity degree thus estimated at each T_{cr} for cold and melt crystallization is plotted in figure 3.8 (red circles), never attaining unity, which means that the final material is not fully crystalline. Nevertheless, a highly crystalline material was obtained at the end of each isothermal crystallization coming from either glassy or molten states as evaluated by the depletion of the dielectric strength of the remaining processes that is much less than 1% of the original magnitude of the main α-relaxation.

Isothermal crystallization was also monitored by POM at some definite temperatures including 221 K. In figure 3.7 the microphotographs taken at the beginning of crystallization (100% amorphous sample) and after 30 minutes were included, the latter clearly showing that the sample is crystalline at the extent of the microscope resolution presenting a uniform grain like morphology.

The fact that the α-relaxation depletes with no changes in the relaxation time can be taken as an indication that the domain size of the cooperative motion underlying the dynamic glass transition is sufficiently small relative to the distance between crystallites, so the growing crystal units do not perturb dipole relaxation.[5, 79] This behaviour was observed also for other non-polymeric materials as ethylenoglycol dimethacrylate,[21] isooctyloxycyanobiphenyl[80] and pharmaceutical drugs.[5] The detection of the secondary process after the vanishing of the cooperative α-relaxation suggests that the molecular motions that are in its origin occur in dimensions below the lengthscale of cooperativity.

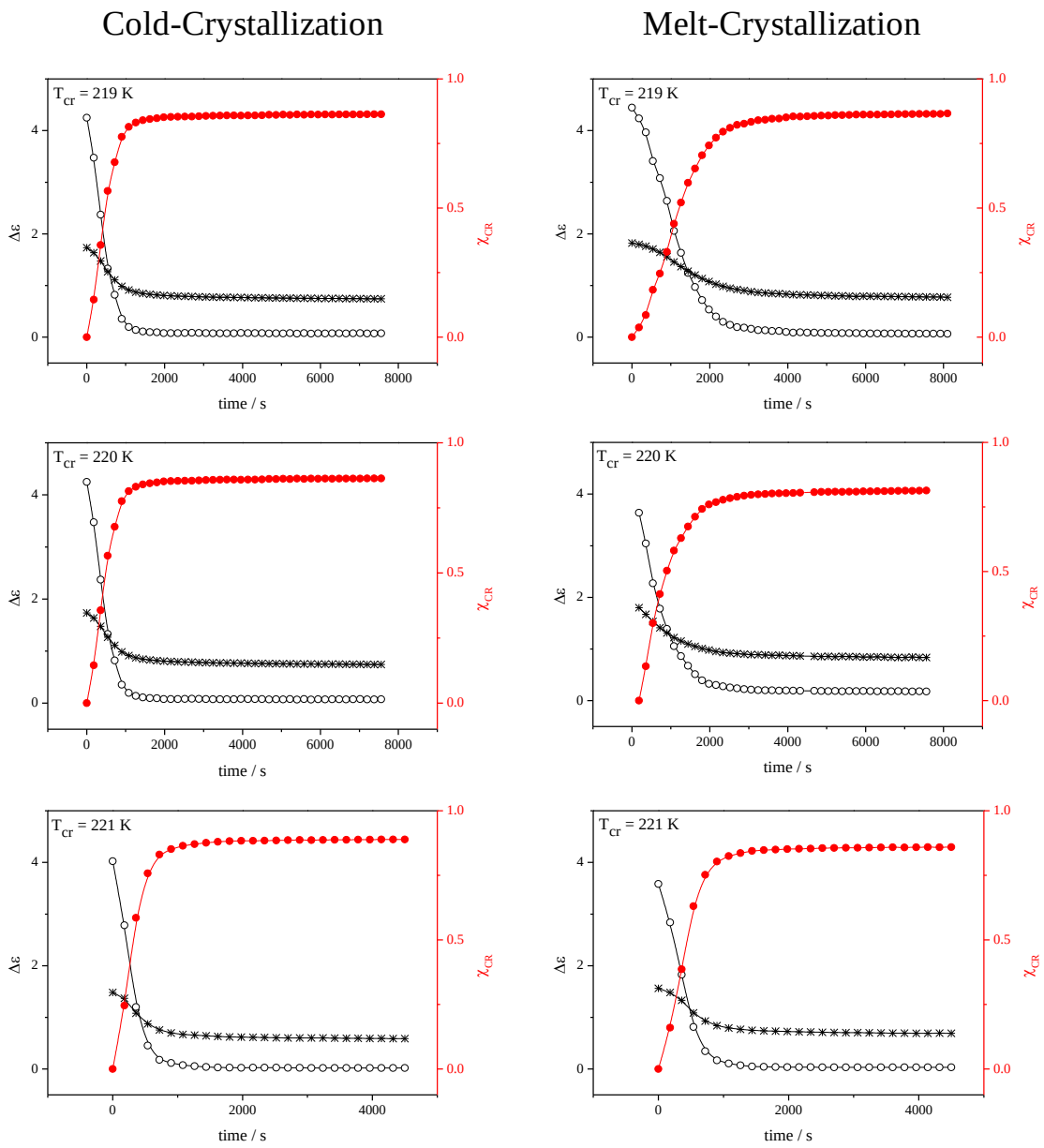

Figure 3.8 Real time evolution of the dielectric strength, Δε, obtained from the fit of a sum of three HN functions to the complex permittivity spectra collected during cold (left plots) and melt crystallization (right plots) at the indicated crystallization temperatures, T_{cr} = 219, 220 and 221 K; open circles correspond to the α-relaxation and crossed circles to the secondary-process (both in the left axis). In the right axis, time dependence of the crystallinity degree, χ_{cr} (filled circles), is reported. Lines are guides for the eye

A common treatment in literature to analyse the transformation from the disordered amorphous into the ordered crystalline phase at a fixed temperature is the Avrami model.[22-24] In this treatment of the isothermal crystallization kinetics, different nucleation and growth mechanisms have correspondingly different time dependences of the crystallization rate that can be modeled by the Avrami law,[22-24] which can be described in terms of the normalized real permittivity, ε'_N. Therefore, to extract kinetic information of Triton X100, the real permittivity at 500 Hz, a frequency for which the low frequency process does not influence the α-process so strongly, was taken and normalized:[19, 71, 81]

$$\varepsilon'_N(t) = \frac{\varepsilon'(0)-\varepsilon'(t)}{\varepsilon'(0)-\varepsilon'(\infty)}$$ Equation 3.3

where ε´(0) is the dielectric permittivity at the start of the crystallization, ε´(∞) the long time limiting value, and ε´(*t*) is the value at the allowed time for crystallization, *t*, figure 3.9 presents the semi-logarithmic plot of ε'_N in function of time at each crystallization temperature; no significant differences were found between the time evolution of the normalized values of both type of crystallizations. For the case of considering ε'_N, the Avrami law reads:

$$\varepsilon'_N(t) = 1 - \exp(-kt^n)$$ Equation 3.4

where *k* is a temperature dependent rate constant, and n the Avrami parameter that can take values between 1 and 7 depending on nucleation type and crystal growth mechanism.[19] A plot of ln[-ln(1-ε´N(*t*))] *vs.* ln *t* gives a straight line having n as the slope and –ln *k* as the intercept (linearization of equation 3.4). The corresponding plot is shown in the inset of figure 3.9 for both type of crystallization. The linearization does not hold for the entire time range, nevertheless for T_{cr}= 219 K it was possible to analyse the linear behaviour at the shortest crystallization times; the obtained n and k values for crystallization carried at 219 K are presented in table 3.4. The almost flat region at longer times at each T_{cr} corresponds to an invariant crystallization degree achieved.

Alternatively, the kinetic analysis can be carried out rewriting the Avrami equation taking in account t0, the induction time preceding crystallization and a characteristic time for the isothermal crystallization, τ_{cr},[22-24, 82]

$$\varepsilon'_N(t) = 1 - exp\left[-\left(\frac{t-t_0}{\tau_{cr}}\right)^n\right]$$ Equation 3.5

where ε'_N(t) is the fraction transformed in the crystalline phase at time (*t*), and τ_{cr} is obtainable from the Avrami parameters by the relationship τ_{cr} = k -1/n. Equation 3.5 is the basis of a modified method of data analysis proposed by Avramov et al [82] which is more sensitive to the changes in the time scale of τ_{cr}, avoiding problems due to a non-correct evaluation of t_0 or lack of thermal stability in collecting the first experimental points.[81]

Figure 3.9 shows the normalized values of the real permittivity for cold and melt-crystallizations carried at the 3 temperatures. To estimate τ_{cr}, t_0 and n, equation 3.5 was directly fitted to ε'_N(t) data corresponding to the solid lines in the Figure; the semi-logarithmic plot enhances the agreement obtained for the shortest times being special sensitive to the value of the induction time. The estimated quantities are included in table 3.4.

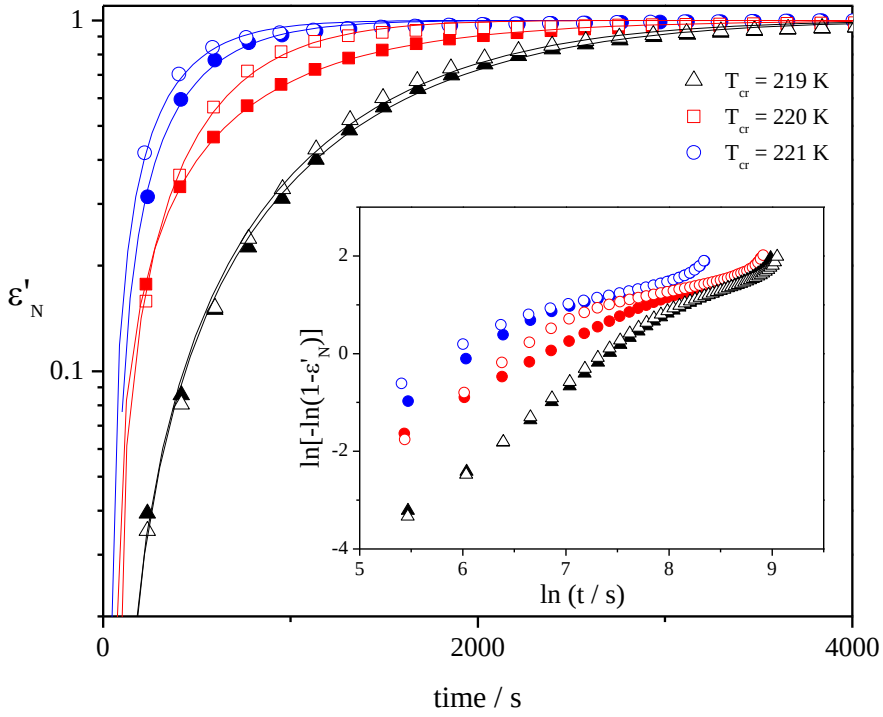

Figure 3.9 Semi-logarithmic plot of the time evolution of the normalized real permittivity, ε'_N, for both cold- (open symbols) and melt-crystallization (filled symbols), evidencing how well eq.3.5 describes data from the initial times; the inset shows the double logarithmic Avrami plot of ε'_N.

Table 3.4 Kinetic parameters obtained from the fit of equation 3.5 to the normalized real permittivity for both melt and cold-crystallizations at each T_{cr}; in the last row: kinetic parameters obtained from the Avrami linearization (double logarithmic plot of $\varepsilon'_N(t)$) taken at the shortest times of both crystallizations carried at 219 K.

	Temperature / K	t_o / s	τ_{cr} / s	k / s^{-n}	n
	Cold-Crystallization				
Avrami equation (eq 3.5)	221	34±10	334±14	(1.5±0.5) x10^{-3}	1.12±0.05
	220	43±17	646±22	(1.7±0.5) x10^{-4}	1.34±0.04
	219	34±27	1596±32	(7±2) x10^{-6}	1.61±0.03
Double ln Avrami Plot	219	--[a)]	(1.6±0.4) x10^{3}	(1.9±0.3)x10^{-6}	1.78±0.02
	Melt-Crystallization				
Avrami equation (eq 3.5)	221	58±16	405±18	(1.2±0.3) x10^{-3}	1.12±0.4
	220	40±7	874±10	(8±2) x10^{-4}	1.05±0.03
	219	39±23	1675±28	(9±2) x10^{-6}	1.57±0.03
Double ln Avrami Plot	219	--[a)]	(1.8±0.4) x10^{3}	(3.5±0.6) x10^{-6}	1.68±0.02

a) the t_0 value cannot be directly determined from the double logarithmic linearization

The n values found are below 2 which in light of the model, could be interpreted as a crystal growth of low dimensionality.

To rationalize this behaviour it is important to understand how crystallization evolves. This phenomenon is usually interpreted in terms of a nucleation/growth process, meaning that the occurrence of crystallization requires the presence of nuclei (nanosize clusters) on which the crystals will subsequently growth (micron-size crystals).[83] For a variety of materials the nucleation rate has a maximum above T_g while the maximum growth rate is further displaced at higher temperatures somewhere between T_g and T_m.[2] The rate of nucleation and growth of the clusters of the newly evolving crystalline phase is dictated by the rate of the diffusion of the ions/molecules that build the crystalline phase.[83] Therefore to allow diffusion to occur it seems reasonable to assume that some segmental motion enabled by the α-process is required, as observed previously by our group for another compound, the EGDMA monomer,[4, 21] which also carries an ethylene glycol moiety. In the latter, the dimensionality achieved by DRS was higher; n was in the range between 1.6 and 3[21] and its onset was always above T_g, $0.87 \leq T_g/T_{cr} \leq 0.92$. In Triton X100 it was observed that crystallization occurred much closer to the glass transition temperature $0.95 \leq T_g/T_{cr} \leq 0.96$. The two features, i) low n values and ii) closeness to the glass transition of crystallization, are coherent with the morphology obtained by POM where a grain like microstrucutre with no optically resolvable spherulites is observed when crystallization was monitored close to T_g. Moreover, for Triton X100 it was found that the crystalline morphology depends on the degree of undercooling, (T_m-T), being observed that shperulites emerge when crystallization is promoted at temperatures between 233 K and 253 K ($24\ K \leq T_m - T \leq 44\ K$); see figure 3.10. A similar dependence of morphology with the degree of undercooling is also reported for PLA[15] and for a semicrystalline polyimide.[84] For the latter it is claimed that the nucleation density increases sharply with small increases in the degree of undercooling, with a concomitant decrease in the spherulitic size, the fine grainy morphology being attributed to a catastrophic nucleation density.[84]

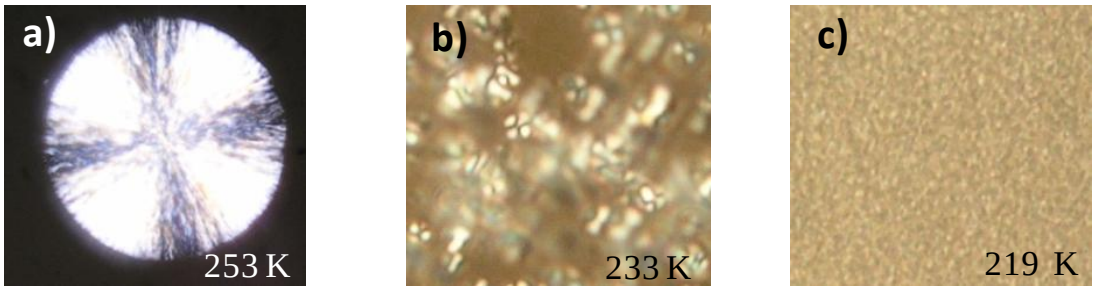

Figure 3.10 Microphotographs taken by POM evidencing the variation of the crystalline morphology with the degree of undercooling (T_m-T_{cr}); the indicated temperatures are the T_{cr} values at which the evolving of crystalline phase was monitored: a) 24 K, b) 44 K and c) 58 K apart from T_m.

3.3 Mobility after Crystallization

At the end of each isothermal crystallization reported in the previous section, the semi-crystalline sample was cooled down to 153 K and successive dielectric spectra were measured while increasing temperature to evaluate the mobility of the remaining amorphous fraction. Figure 3.11 presents the collected spectra for T_{cr}=219 K at some representative temperatures (see legend). Comparing with the spectra taken for the full amorphous material (Figure 2.1) the main differences are the suppression of the cooperative α-process and a better definition of the β-relaxation. From the HN fit (equation 1.11, see *Introduction* section 1.5) to the raw data a relaxation map was built for the semi-crystalline material shown in figure 3.12.

Figure 3.12 shows that the Arrhenius plot for the relaxation times of the secondary γ-process detected in the semi-crystalline material (γ_{sc}) almost superimposes the one of the full amorphous material (black diamonds *vs* gray diamonds), giving an activation energy of 35.6±0.2 kJ·mol^{-1}; this value is in good accordance with the value estimated for the full amorphous material (36.4±0.1 kJ·mol^{-1}). In spite of a slight decrease in its relaxation strenght, the secondary γ_{sc}-process keeps the same characteristics of the full amorphous process (γ_{am}) as shown by the coincidence of normalized plot in the inset for the spectra collected at 153 K.

In regard to the β-relaxation, as already mentioned, it was possible to resolve this process in a wider temperature range obtaining similar activation energy (solid line in the figure) for both semi-crystalline and amorphous materials; $E_{a(\beta sc)}$ =75 ± 5 kJ·mol^{-1} close to the previous estimated value for the amorphous Triton X100, 82 ± 1 kJ·mol^{-1}.

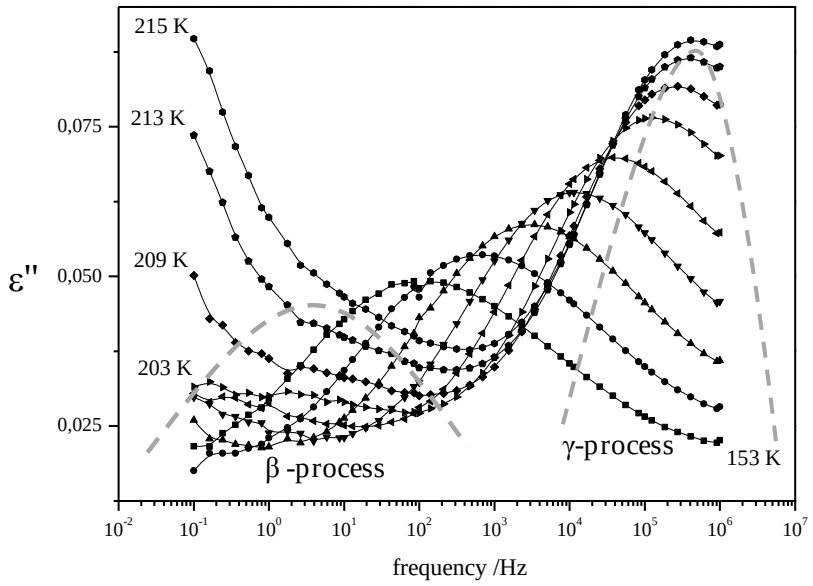

Figure 3.11 Dielectric loss versus frequency after isothermal cold-crystallization at 219 K for temperatures between 153 K and 203 K in steps of 10 K and at 209 K, 213 K and 215 K.

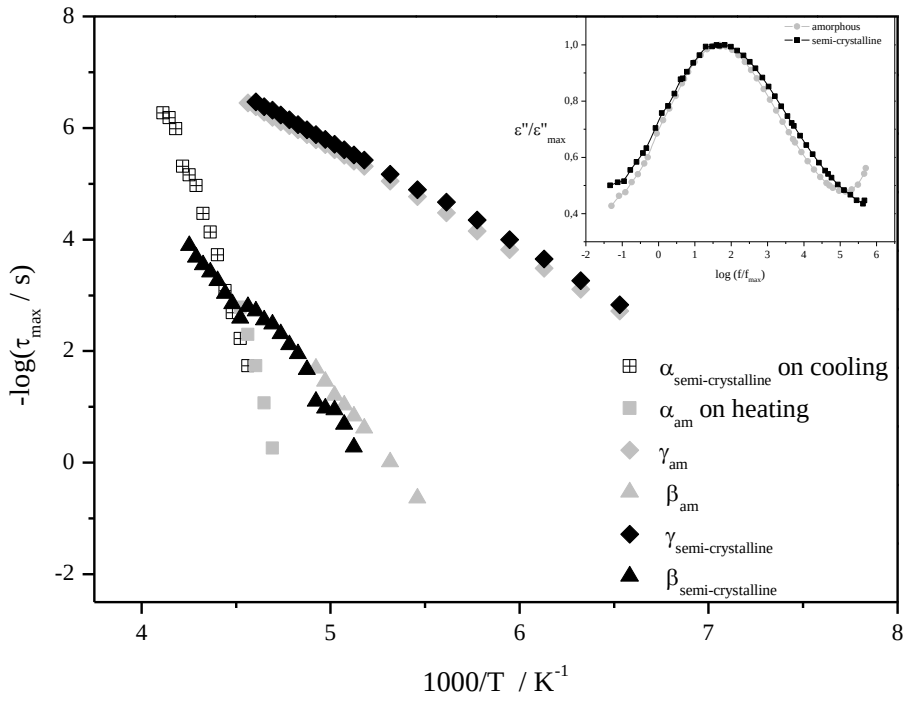

Figure 3.12 Relaxation map of all detected processes for the full amorphous sample ($_{am}$) and after crystallization at 219 K ($_{sc}$ - semi-crystalline); the solid lines are the Arrhenius linear fit. While the relaxation times for the secondary processes were estimated from measurements done after isothermal crystallization, the τ values for the α-process ($_{sc}$) on cooling were obtained after non-isothermal molten crystallization. The inset presents the normalized plot for the dielectric loss of the γ-process at 153 K for the amorphous and semi-crystalline sample.

The relaxation map (figure 3.12) also includes the relaxation times for the α-process obtained from measurements during which non-isothermal molten crystallization occurred (blue squares). It is obvious that the α-process is still active nevertheless the respective τ values are slightly shifted towards higher values (slower mobility); even so the glass transition temperature estimated from dielectric data at τ =100s (209 K) agrees with the T_g value for the bulk. Although not shown, the remaining α-process in this semi-crystalline material comes highly depleted; the area of the α-peak after crystallization depletes more than one decade relative to the area of full amorphous Triton X100 allowing to roughly estimating the crystallization degree as more than 90%; in the next section this will be further analysed.

The dynamical behaviour after isothermal crystallization carried at 219 K is similar for the material after being crystallized at 220 and 221 K. This becomes evident from the ε´´ plot taken at a fixed frequency (10^4 Hz) in function of temperature (isochronal plot) shown in figure 3.3. The three ε_{10kHz}´´(T) plots almost fall in a single chart confirming that the mobility of the amorphous fraction that remains in the material after crystallization at each T is identical.

The figure also includes the isochronal plot for the full amorphous material and the one taken after isothermal crystallization carried at 251 K. For the latter it is obvious the detection of the α-relaxation even after 2,5 hours under crystallization. This temperature was chosen to monitor crystallization since it was one at which well optical resolved shperulites emerge, as seen by POM (remember figure 3.10 a). From this figure it becomes evident how the thermal history influences the dynamical behaviour of the material.

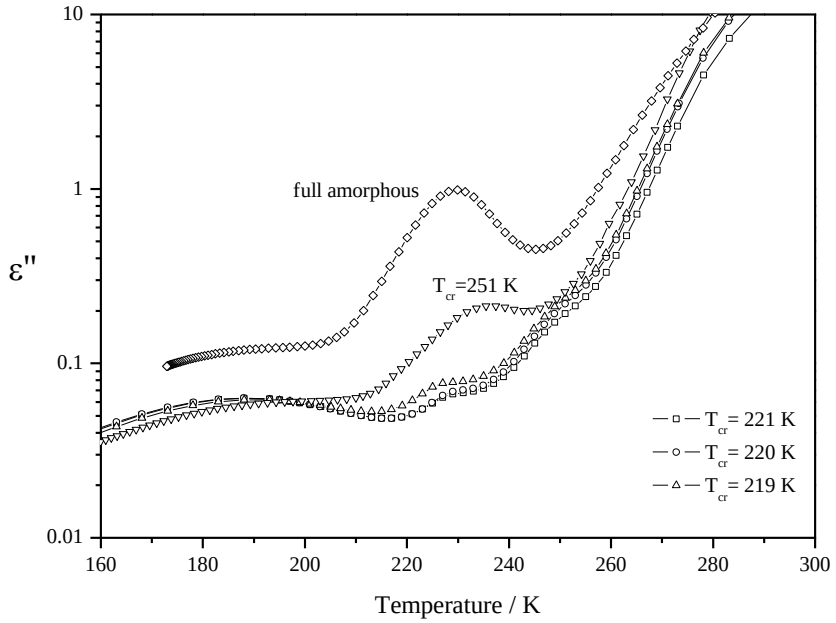

Figure 3.13 Imaginary part of the complex permittivity in function of temperature illustrating the influence of thermal history in the dynamical behaviour of the material

3.4 Dynamical behaviour under confinement

In line with the influence of the thermal history on the dynamical behaviour of Triton X100 evaluated in the last section, now the effect of confinement to nanodimensions will be analysed. This study is interesting because the Triton X100 is a glass-former and investigated the effects that occurs in the glass transition when it is confined can provide additional information on the dynamics of glass transition and may help to check theories and models proposed for it.[85]

As mentioned in the Experimental Section, Triton X100 was impregnated in a nanoprous matrix, silica based, designated as SBA-15 with an average pore diameter of 5.7 nm. The evaluation of the impregnation efficiency and an initial study about the molecular mobility of the Triton X100 confined in SBA-15 are carried out using different techniques.

In the last part, a comparison of the results obtained by DRS for the Triton X100 confined in SBA-15 and confined in another nanoporus guest are show.

3.4.1 Composition and thermal analysis of Triton X100 confined in SBA-15

3.4.1.1 ATR-FTIR

To evaluate if a successful loading of Triton X100 in SBA-15 was achieved, ATR-FTIR (see Experimental Section) was used. The spectra thus collected are compared in figure 3.14: unloaded SBA-15(blue line) and SBA-15 Triton X100 loaded (red line), and bulk Triton X100 (black line); please remember that unloaded SBA-15 was submitted to the same treatment then the loaded matrix using ethanol.

Two main regions give the evidence of a successful loading: i) one at a wavenumber of 1512 cm^{-1} assigned to a coupling of aromatic ring C-C stretching and C-H deformation modes in Triton[86], (see a scale up in the upper inset) and ii) a band near 3000 cm^{-1} due to C-H stretch (dashed circle). Both absorptions are absent in the spectrum of the empty matrix.

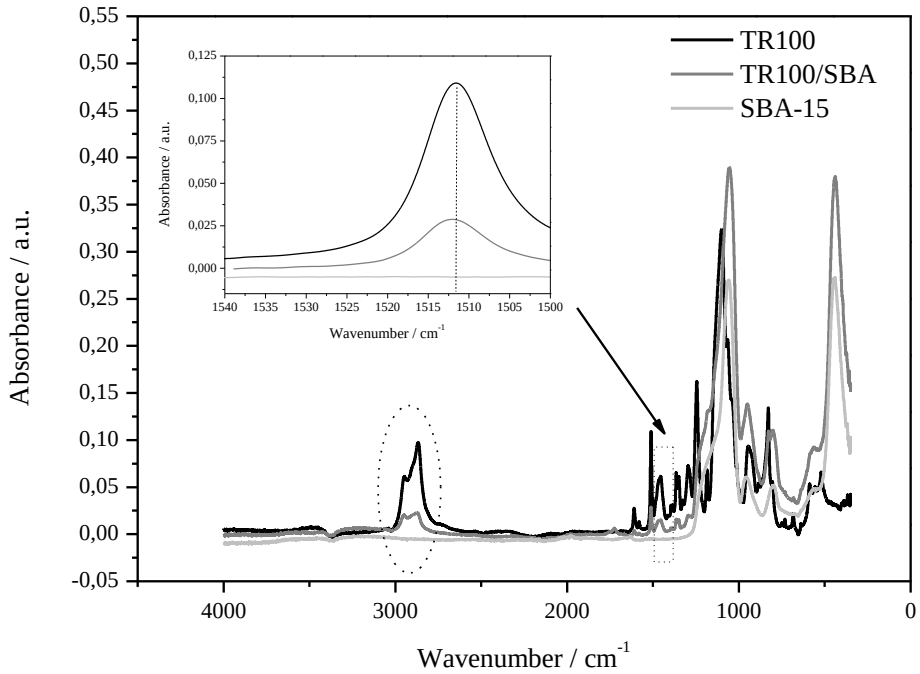

Figure 3.14 ATR-FTIR spectra of TR100/SBA compared with Triton X100 bulk and unloaded SBA-15 at room temperature. The inset presents the ATR-FTIR spectra in the frequency region of C-C stretching. The dashed circle indicates the region of the spectrum due to the C-H stretch of Triton X100.

3.4.1.2 TGA

To quantify the amount of loaded Triton X100, thermogravimetric analysis (TGA) was carried out (see *Materials and Methods* section 2.3.4); see Figure 3.15. From the weight loss due to the burning and decomposition of the guest molecules, measured up to ca. 1073 K, the Triton X100 loading was estimated as ~50%; the thermogram exhibits two steps which will be commented further on. It was verified that the mesoporous matrix is thermally stable up to temperatures above 1000 K (after a small

initial lost weight due to water/solvent removal, its weight is constant by increasing the temperature up to 1073 K). In the loaded matrix the initial drop due to water/solvent evaporation is negligible (< 1%).

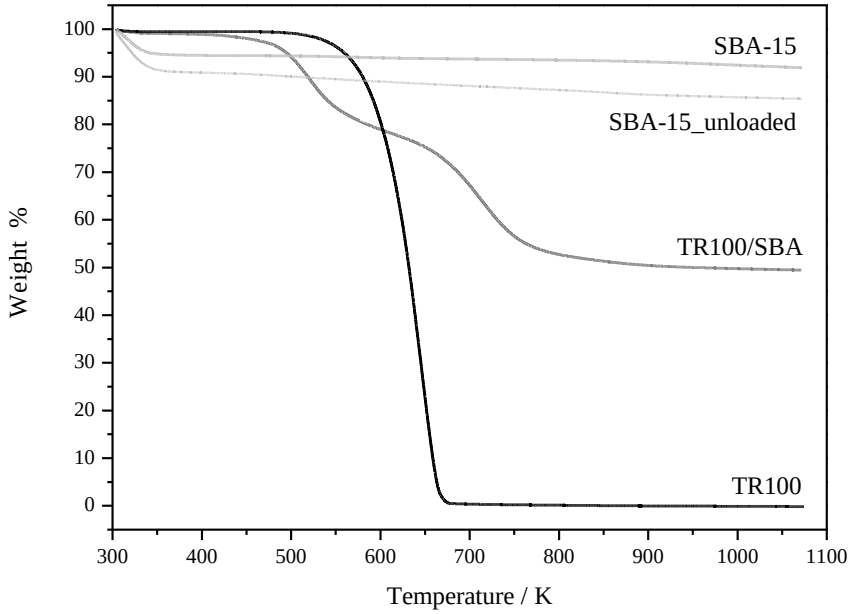

Figure 3.15 Thermogravimetric curves obtained on heating at 10 K·min^{-1} for the mesopores SBA-15 (as prepared), SBA-15 unloaded and loaded with Triton X100 (TR100/SBA) and bulk Triton X100.

The two methods reported above give indication that a successful loading of Triton X100 was achieved.

3.4.1.3 DSC

Differential scanning calorimetry measurements were was also carried out for the unloaded and loaded matrix and compared with bulk Triton X100. The respective thermograms are shown in figure 3.16.

The shadow areas indicate the transitions detected in the loaded SBA15 which are also observed for the neat constituent: the gray area corresponds to the glass transition of Triton X100 (vertical bar points to the midpoint of the glass transition 218.15 K *vs* 214.15 K in bulk Triton X100); the blue area indicates the thermal response of the unloaded SBA-15 which, even after heating up to 373.15 K, is still detected (2nd run). The thermogram for the confined system does not exhibits the crystallization exothermal observed for bulk Triton X100 (~230 K), neither the endothermic melting, meaning that the guest do not undergo crystallization. This behaviour is reproducible in subsequent runs.

Interesting enough is the detection of a second step in the heat flow, immediately after the bulk-like glass transition of Triton X100 in the composite, with a midpoint located at 236.18 K (2nd vertical bar). Therefore, DSC give a further evidence of impregnation, however to get a further insight in the behaviour of the confined guest, dielectric relaxation spectroscopy was carried out and described in the next section.

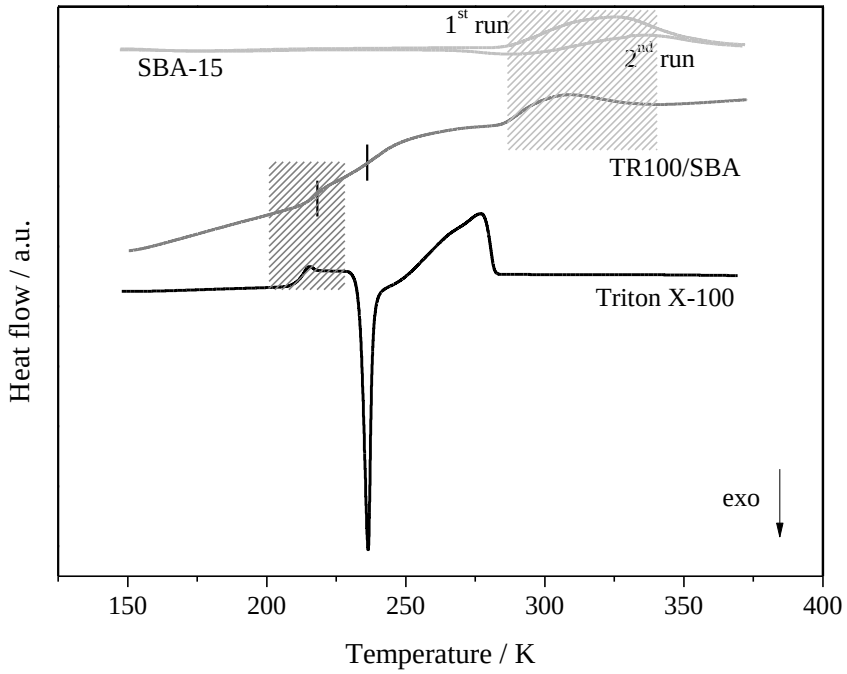

Figure 3.16 Thermograms (heat flow in arbitrary units a.u., *vs* temperature) of the unloaded and loaded SBA-15 matrix and of bulk Triton X100; the curves were vertically displaced to make the comparison easier. The shadow areas indicated the thermal events common to the composite and neat constituents. The vertical bars indicate the midpoint of the heat flux jump in the two detected glass transition regions for confined Triton X100.

DRS measurements were taken from 153 to 393 K for SBA-15 impregnated with Triton X100. Dielectric measurements were cooled isothermally increasing the temperature in different steps, from 153 K to 193 K in increasing steps of 5 K and from 195 K to 273K the dielectric spectra were recorded every 2 K; in the remaining temperature region the spectra were recorded every 5 K. (see *Materials and Methods* section 2.3.2)

3.4.2 Dielectric studies of the Triton X100 confined

Figure 3.17 presents the isochronal plots of the real (a) and imaginary (b) parts of the complex permittivity at different frequencies and figure 3.18 compares the behaviour for the loaded matrix with the unloaded one and bulk Triton X100 at $f = 10^4$ Hz.

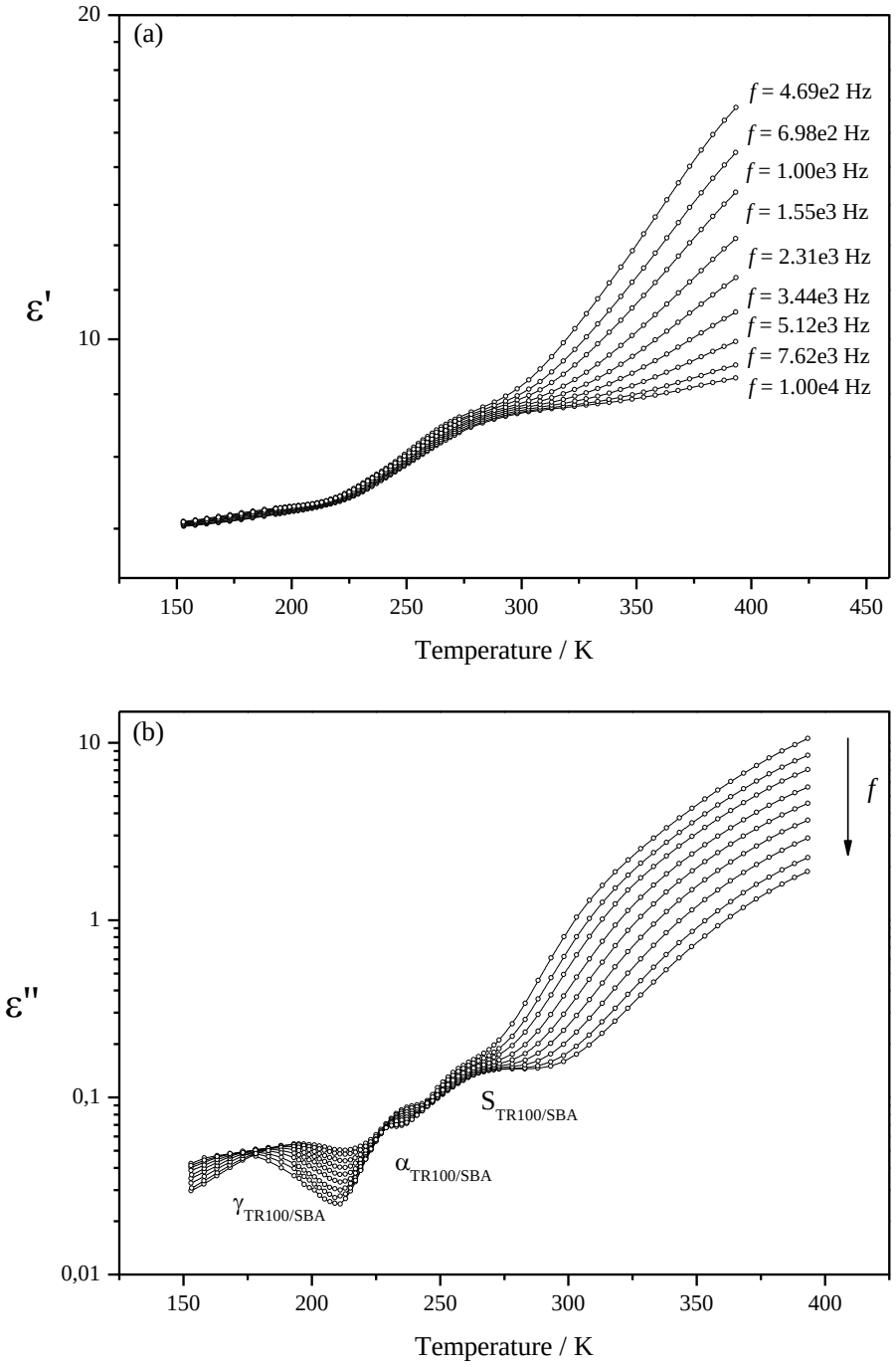

Figure 3.17 Temperature dependence of the complex permittivity (a) real and (b) imaginary part at some representative frequencies collected upon isothermal measurements.

It must be noted that the dielectric loss of the dried SBA-15 matrix is negligible small compared to that observed for the filled matrix (figure 3.18); therefore the detected dielectric response for the TR100/SBA composite is due to Triton X100 giving further evidence that it is confined into the nanoporous host.

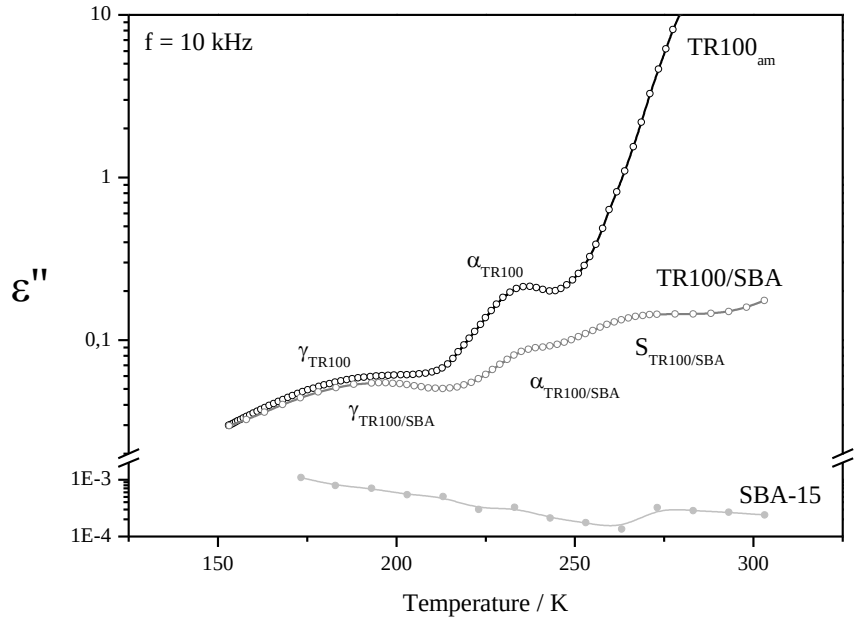

Figure 3.18 Dielectric loss of confined Triton X100 *vs* temperature at a frequency of 10 kHz compared with bulk Triton X100 and SBA-15 matrix. The dashed line indicates the assignment of the detected process in the composite to the dynamic glass transition observed in bulk Triton X100.

A multimodal character for both ε´and ε´´ traces is found. The comparison with bulk Triton X100 allows assign the detected processes: the one located at the lowest temperatures being the γ-process followed by a bulk-like α-relaxation. At this frequency (10 kHz), the α-relaxation seems to be located at the same temperature then for bulk Triton X100; however, the comparison at different frequencies leads to conclude that this process in the confined guest is slightly shifted to higher temperatures. This was also found in DSC measurements where a shift of ~5K towards higher temperatures was detected for the confined Triton X100 meaning that the molecular guest under confinement is slightly less mobile. In addition another relaxation process is detected at higher temperatures relative to this bulk-like α-process. A similar process was observed for confined guests interacting with the pore surface of the host having a slower dynamics[7, 59, 87, 88] being designated as surface process (S). It was already observed by some of us for Ibuprofen impregnated in the same SBA-15 porous matrix.[7] This was attributed to the guest Ibuprofen molecules interacting via hydrogen bonds with the silica groups of the matrix. In the present system an equivalent interaction could occur between the OH terminal group of Triton X100 and the Si-OH groups present in the pore wall. Therefore, this S process in confined Triton X100 is assigned to the surfactant molecules localized close to the pore walls and interacting with the surface silanol groups. Moreover, in Ibuprofen/SBA system and also in E7 impregnated in the same porous host, the S process is the dominant one as found here for confined Triton X100.

To investigate in detail the different relaxation processes for the Triton X100 confined, the isochronal representation of the dielectric loss, ε´´ *vs* temperature at constant frequencies (ε´´(T; *f* = const)) is now analysed. Hence, the dielectric loss can be described as a superposition of k Gaussians functions and obtain the maximum temperature of peaks, T_{max}, for some of the frequencies measured. This method has also been proved to be advantageous when the multiple relaxation process present a response very low making very difficult the analysis of dielectric loss spectra in the frequency domain.[7, 89]

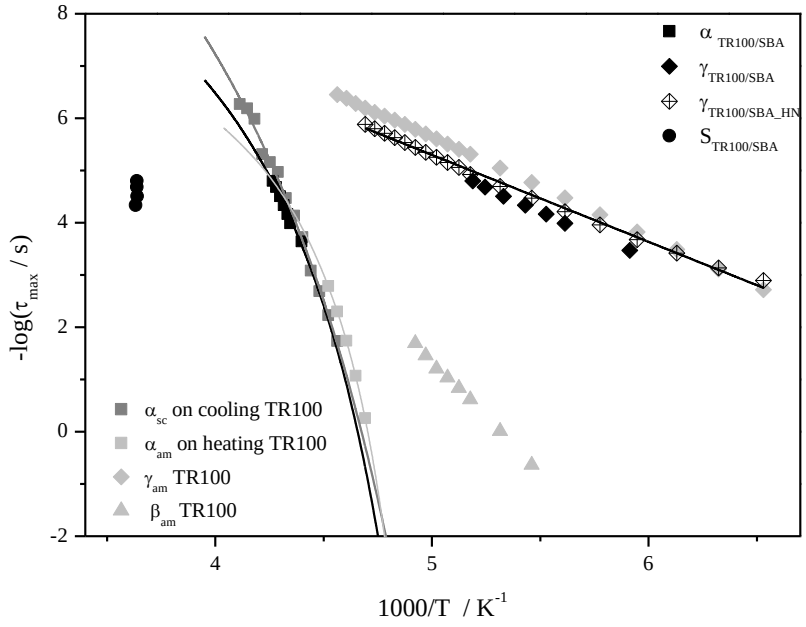

Figure 3.19 Relaxation map of all detected processes for the confined system TR100/SBA (black symbols); the relaxation times for the full amorphous ($_{am}$) and semi-crystalline ($_{sc}$) material were also included for comparison. The lines are fits of the Arrhenius and VFT formulas to the corresponding data

Figure 3.19 shows the temperature dependence of the relaxation time τ obtained from the isochronal plots (τ = 1/(2πf), $1/T_{max}$) for the confined Triton X100. For the secondary γ-process that emerges relatively well defined, it was possible to fit ε´and ε´´ curves obtained from the isothermal measurements by the HN equation. Therefore, the thus estimated relaxation times are also included in the relaxation map (crossed losanges) and the solid line is the respective Arrhenius fit. In addition, the relaxation times for bulk Triton X100 extracted from the HN-fitting were included. The parameters of the individual functions used to the fit the different process are summarized in table 3.5.

The confined Triton X100 exhibits three different relaxation processes: a secondary γ-process, the main α –relaxation and a surface relaxation process, in order of increasing temperature.

At lower temperatures, the results clearly show the presence of one secondary relaxation which is also detected in the bulk Triton X100, the γ-process. Nevertheless, this process has slight different

activation energy. While the raw data curves superimpose (in location) at the lowest temperatures, for temperatures higher than 173 K the confined guest has slower mobility (higher relaxation times) giving rise to a lower value of activation energy (31.8±0.5 kJ·mol^{-1}).

The β-process observed both in the amorphous and semi-crystalline Triton X100 although felt in the isotherms of the confined system, is not possible to extract unequivocally from the raw data, therefore no value is provided for this relaxation.

Concerning the $\alpha_{TR/SBA}$-process, it is interesting to verify that it relaxation times superimpose those estimated for the semi-crystalline state presenting also some curvature as characteristic of a cooperative process. This means that the mobility of the confined guest is similar to that of the amorphous material constrained between the crystalline phases. These results indicate that for the confined Triton X100, the dynamics of the glass transition becomes relatively slower and the glass transition temperature estimated from dielectric data (τ = 100s) slightly increases (~1.5 K) compared to the bulk. The shift of the glass transition temperature towards an higher value is in agreement with the DSC results for which an increase of 4 K was found; these results are coherent with the observations reported by Schüler *et al* [90] for confined proylene glycol and its oligomers that found an increase of 4.5 K for the glass transition temperature compared to bulk.

At higher temperatures (lower relaxation times) then $\alpha_{TR/SBA}$-process, the dominant S-process is observed for the confined system however the few data point do not allow a reliable fit; for a more detailed discussion further studies are needed.

The simultaneous observation of an α-relaxation and a S-process, allows to classify the dynamics of confined Triton X100 molecules into two fractions: one liquid-like due to molecules close to the pore centre with relaxation rates close to the bulk guest and another due to molecules interacting with the pores with reduced mobility; this was also observed in Ibuprofen and the liquid crystalline mixture E7 in SBA-15.[7, 87] The S-process gives rise also to a glass transition process as detected by DSC with an higher T_g value ($T_{g,S}$ 18 K above $T_{g,\alpha TR100/SBA}$). The two step profile in the loss weight curve observed by thermogravimetry also points into this direction: the molecules interacting with the surface are the ones that decompose at higher temperatures.

Table 3.5 Summarizes the activation parameters for all detected processes in the different conditions investigated here.

		Bulk TR100	**Semi-crystalline TR100**	**TR100/SBA**
α-process	**Ea(Tg) / kJ· mol^{-1}**	590.8	373.3	468.3
	τ_∞/ s	1.1 x 10^{-09}	3.1 x 10^{-17}	1.34 x 10^{-12}
	T_0 / K	193.6	167.5	185.4
	T_g (τ=100s) / K	209.1	208.9	210.5
γ-process	**E_a / kJ· mol^{-1}**	36.4	---	31.8
	τ_∞ / s	7.5 x 10^{-16}	---	1.4 x 10^{-14}

To finalize, it is interesting to analyse another effect of confinement regarding the influence of thermal treatment. While bulk Triton X100 crystallizes during measurements at a low cooling and/or heating rate, for the confined guest crystallization was never observed. Figure 3.20 compares the absence of crystallization in the confined material when is submitted to the same thermal treatment that the Triton X100 bulk. The (ε´(T)) trace for the bulk material illustrates the typical profile when crystallization occurs by the sudden drop at around 225 K. The nonexistence of discontinuity in the ε´ trace, upon cooling and subsequently heating, for the TR100/SBA confirmed that the crystallization is circumvented in the confined Triton X100. This behaviour is reproducible, confirming that confinement is a good strategy to avoid crystallization.

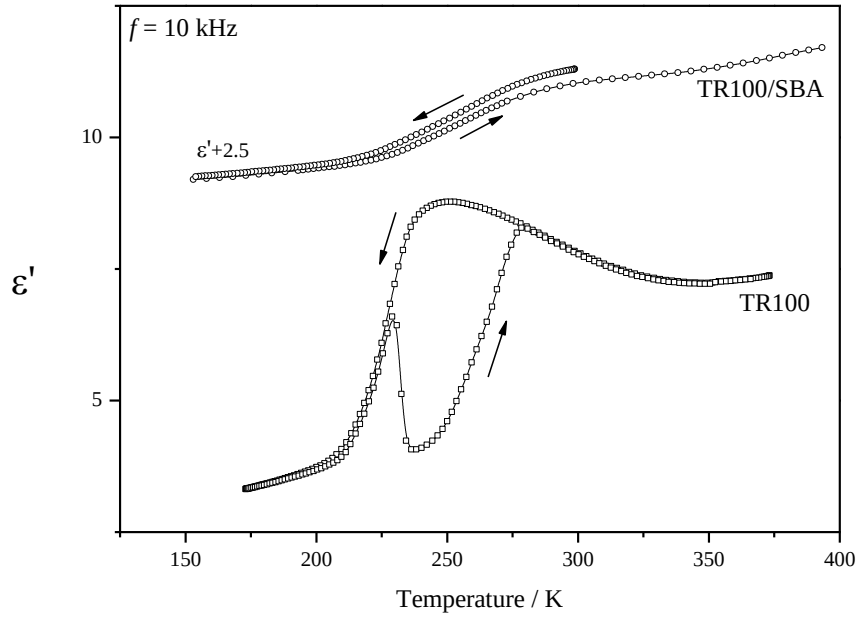

Figure 3.20 Temperature dependence of the real part of the complex dielectric function (ε´(T)) for TR100/SBA and Triton X100. The (ε´(T)) trace for the bulk material illustrates the typical profile when crystallization occurs by the drop in this property (here observed at ~225 K) absent for TR100/SBA confined. Run_1 (down arrows): ramp at a cooling rate of 11 $K \cdot min^{-1}$ for both Triton X100 and TR100/SBA; Run_2 (up arrows): ramp at an heating rate of 9 $K \cdot min^{-1}$ for Triton X100 and isothermal measurements upon increasing different temperature steps (see *Experimental conditions* section 3.2.1.2). For a better clarity the (ε´(T)) values for the confined system were vertically shifted by adding a factor of 2.5.

3.4.3 Triton X100 confined in another porous host.

In order to achieve a better understanding about the effect that the host (pore size, molecular architecture, pores composition) has on the molecular mobility of confined Triton X100, a preliminary dielectric spectroscopy study of the guest confined in another nanoporous matrices was carried out (for information about the materials see *Materials and Methods* section 2.2 and *Appendix II*).

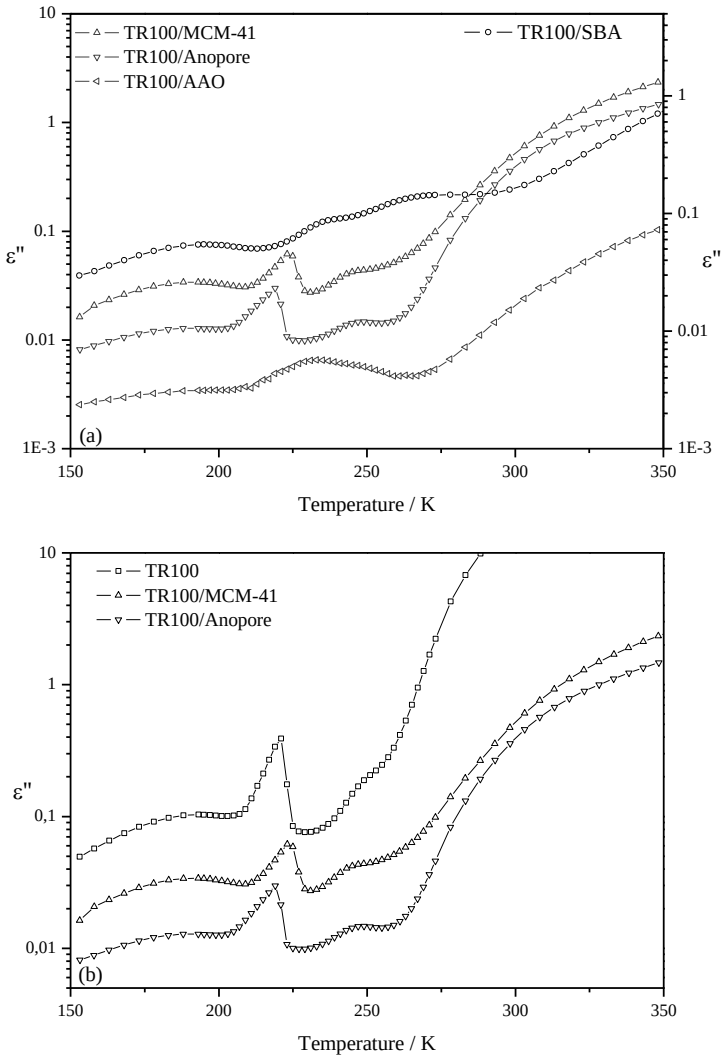

Figure 3.21 Isochronal dielectric loss at 10k Hz in logarithmic scale illustrating the dielectric behaviour of the Triton X100 confined in: SBA-15, MCM-41, Anopore and AAO.

The figure 3.21 (a) compares the dielectric loss for Triton X100 confined in different host versus temperature at fixed frequency (isochronal plot), also illustrating the multi modal character of the spectra. The secondary relaxation, γ, shows up in all the confined systems. For the Triton X100 confined in both, MCM-41 and Anopore, the sharp drop around 223 K and 221 K respectively, in the ε´ trace indicates that crystallization is not avoided. However the molecular mobility is changed compared to that of Triton X100 bulk: this is illustrated in the Figure 3.21 (b) by comparing the dielectric response of TR100/MCM-41 and TR100/Anopore with the bulk. A shift towards high temperatures of the alpha process is observed for confined Triton X100. The Triton X100 confined in AAO show a different response that requires a more detailed study; nevertheless it is clear that crystallization is avoided when Triton X 100 is confined in this matrix.

The results obtained by broadband dielectric give indications that Triton X100 has a different mobility in confinement; moreover the molecular mobility seems to be sensitive to the pore size or to the characteristic/composition of the host system.

Chapter IV: Conclusions

Triton X100, studied in detail in this thesis, is a typical glass-forming with a high response to the electric field in the analysis of DRS. Which allowed us to make both different studies, one about phase transformations undergone by Triton X100, already published and another about the molecular mobility of the Triton X100 bulk and confined in a nanoporous host SBA-15, to be publish in the future.

Temperature driven phase transformations undergone by the surfactant Triton X100 were investigated by DSC and DRS and complemented by POM. The crystallization of the Triton X100 can be easily avoided if the material is cooled at a rate $\geq$10 K·min^{-1}. This means that under these specific conditions, it is possible to enlarge ~60 K the temperature range where TritonX-100 exhibits liquid and supercooled liquid properties, with vitrification occurring only around 206 K.

A complete dielectric characterization of Triton X100 in the glassy supercooled and molted is provide covering a broad frequency range. The results show that the relaxation map including two secondary processes (γ and β) associated with the local mobility and the process associated to the glass transition (α), influenced by the cold-crystallization.

Temperature-driven phase transformations undergone by the surfactant Triton X100 were investigated by DSC and DRS and complemented by POM.

For cooling rates under 10 K·min^{-1}, crystallization is always observed, emerging at temperatures that are higher the lower is the cooling rate. When the material is cooled at a rate $\geq$5 K·min^{-1}, cold-crystallization is always observed upon subsequent heating.

It was observed by POM that the attained morphology upon crystallization depends on the undercooling degree. In the proximity of the glass transition, for the highest undercooling degree ($T_m - T_{cr} \approx 57$ K), a grain-like morphology is detected, while large and more perfect spherulites emerge for lower undercooling degree (24 K $\leq T_m - T_{cr} \leq$ 44 K).

The evolution of the dielectric α-process and secondary relaxation were followed during cold- and melt-crystallization at T_{cr} = 219, 220, and 221 K, near the glass transition, with no significant changes in either the position or the shape. The secondary relaxation observed in the high frequency flank of the α-peak still persists even when the complete depletion of the α-relaxation was observed.

From the time evolution of the normalized real permittivity, kinetic parameters were extracted considering a modified Avrami law taking into account the induction time. The reason that isothermal crystallization occurs to a great extent in the vicinity of the glass transition was attributed to the occurrence of catastrophic nucleation/crystal growth probably enabled by a preordering tendency of the surfactant molecules.

The ability of Triton X100 to undergo vitrification and crystallization coming from the molten state or from the glass makes it a model compound to investigate temperature-driven phase transformations.

Motivated by the recent knowledge that molecular mobility and phases transformations can be significantly altered when a glass-forming liquid is confined in the nanometer scale, the molecular dynamics of the TRX-100 was evaluated when confined in SBA-15, with a pore size of 5.7nm. The evaluation of the impregnation efficiency was carried out using TGA, ATR-FTIR and DSC.
TGA measurements allowed obtaining the respective filling degrees which are around 50%. Moreover, ATR-FTIR confirmed the existence of two main regions one at a wavenumber of 1512 cm^{-1} assigned to a coupling of aromatic ring C-C stretching and C-H deformation modes in Triton and a band near 3000 cm^{-1} due to C-H stretch intermolecular hydrogen bonded associations for both confined give the evidence of a successful loading.
In the DRS spectra of Triton X100 confined, multiple relaxation processes emerged and revealed a significant variation from the dynamical behaviour of bulk. The relaxation map including one secondary relaxation, γ, a main bulk-like α-process associated with the dynamic glass transition, and a S-process assigned to the Triton X100 molecules adsorbed at the internal pore wall; data relative to the β-process are not provided because is not possible to extract it unequivocally from the raw data. These results and the observation by DSC of two glass transitions for the Triton X100 demonstrate the existence of two families of molecules with different molecular mobilities: one family, due to an interfacial layer formed close to the pore wall, *i.e*. molecules absorbed at the walls, and another family due to the confined liquid consisting in molecules located more in the centre of the pores.

Appendixes

Appendix I

Aluminum Oxide Membranes

Contrary to the above mentioned host materials that were prepared specifically for this word, the aluminum oxide membranes were commercially supplied and provided by a collaborator. These high-purity Al_2O_3 matrixes are able to be prepared with pore sizes in the order or the nanometre. They are a self-organized nanostructured material containing a high density of uniform cylindrical pores that are aligned perpendicular to the surface of the materials making them adequate as host material for confinement studies.

1. Anopore membranes (Anopore)

The Anopore™ inorganic membrane was supplied by Whatman[91] (Anodisc 25, catalogue number 6809-6002) with cylindrical pores of 20nm being provided as 25 mm diameter discs with an average thickness of 60 µm.

2. Aluminum Oxide subtrates (AAO)

Membranes inorganic of AAO were provided by the research A. I. Smirnov. Figure II.1 evidences the uniformity in the pore size (46,461 nm) and the perpendicular alignment of the cylindrical pores to the surface (inset).

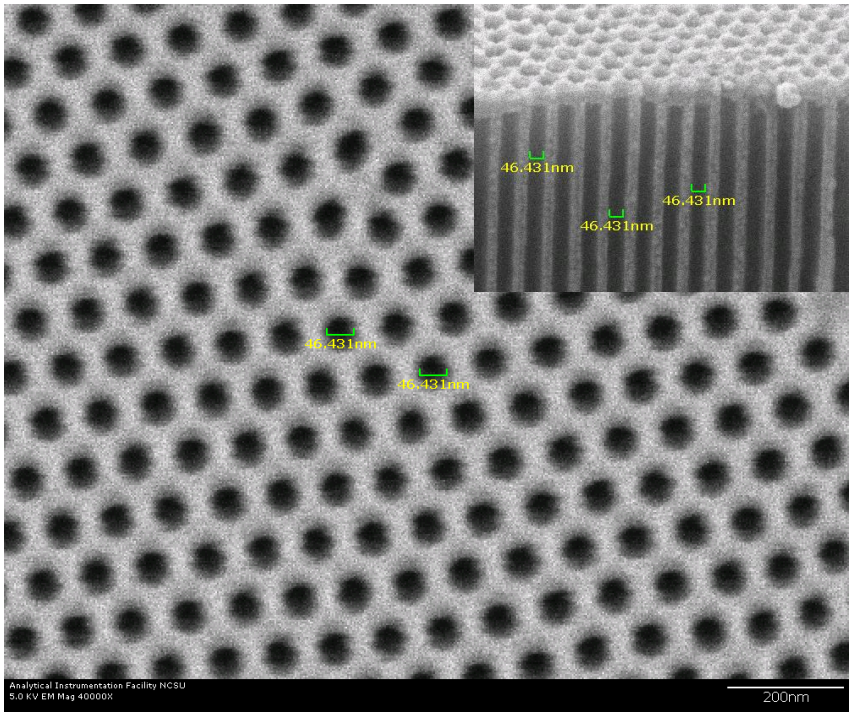

Figure I.1 SEM image clearly showing the uniformity in the pore size (46,461 nm) and the perpendicular alignment of the cylindrical pores to the surface (inset).

Impregnation protocol:

The AAO membranes , Anopore and AAO, were outgassed in vacuum of 10^{-4} mbar at 393 K for 6 h to remove water and other impurities. Then the membranes were slowly cooled down to T=323 K. A solution of Triton X-100 in ethanol (Panreac) was added slowly (drop wise) to the top surface of the membrane. The pores were filled by capillary wetting at room temperature for 12 h. Then, the membranes were dried in filter paper to eliminate the excess of solution and dried under vacuum at 358 K for 6h. The samples were kept in a dessicator.

The amount of TRX-100 with which the different solutions for impregnation were prepared, corresponds to twice the value estimated from the total pore volume for completely loading. This was done to ensure a high degree of filling.

References

(1) Carpentier, L.; Decressain, R.; Desprez, S.; Descamps, M., Dynamics of the amorphous and crystalline alpha, gamma-phases of indomethacin. *Journal of Physical Chemistry B* **2006,** 110, (1), 457-464.

(2) Andronis, V.; Zografi, G., Crystal nucleation and growth of indomethacin polymorphs from the amorphous state. *Journal of Non-Crystalline Solids* **2000,** 271, (3), 236-248.

(3) Vallet-Regi, M.; Granado, S.; Arcos, D.; Gordo, M.; Cabanas, M. V.; Ragel, C. V.; Salinas, A. J.; Doadrio, A. L.; San Roman, J., Preparation, characterization, and in vitro release of ibuprofen from Al2O3/PLA/PMMA composites. *Journal of Biomedical Materials Research* **1998,** 39, (3), 423-428.

(4) Viciosa, M. T.; Correia, N. T.; Sanchez, M. S.; Ribelles, J. L. G.; Dionisio, M., Molecular Dynamics of Ethylene Glycol Dimethacrylate Glass Former: Influence of Different Crystallization Pathways. *Journal of Physical Chemistry B* **2009,** 113, (43), 14196-14208.

(5) Alie, J.; Menegotto, J.; Cardon, P.; Duplaa, H.; Caron, A.; Lacabanne, C.; Bauer, M., Dielectric study of the molecular mobility and the isothermal crystallization kinetics of an amorphous pharmaceutical drug substance. *Journal of Pharmaceutical Sciences* **2004,** 93, (1), 218-233.

(6) Bohmer, R.; Ngai, K. L.; Angell, C. A.; Plazek, D. J., Nonexponential relaxations in strong and fragile glass formers. *Journal of Chemical Physics* **1993,** 99, (5), 4201-4209.

(7) Bras, A. R.; Merino, E. G.; Neves, P. D.; Fonseca, I. M.; Dionisio, M.; Schoenhals, A.; Correia, N. T., Amorphous Ibuprofen Confined in Nanostructured Silica Materials: A Dynamical Approach. *Journal of Physical Chemistry C* **2011,** 115, (11), 4616-4623.

(8) Frunza, S.; Frunza, L.; Schonhals, A., Dielectric measurements of liquid crystals confined to molecular sieves. *Journal De Physique Iv* **2000,** 10, (P7), 115-118.

(9) Schonhals, A.; Goering, H.; Schick, C., Segmental and chain dynamics of polymers: from the bulk to the confined state. *Journal of Non-Crystalline Solids* **2002,** 305, (1-3), 140-149.

(10) Kremer, F.; Huwe, A.; Schönhals, A.; Rózanski, S. A., Molecular dynamics in confining space. In *Broadband Dielectric Spectroscopy*, Kremer, F.; Schönhals, A., Eds. Springer: Berlin, 2003.

(11) Yuan, H. Z.; Cheng, G. Z.; Zhao, S.; Miao, X. J.; Yu, J. Y.; Shen, L. F.; Du, Y. R., Conformational dependence of triton X-100 on environment studied by 2D NOESY and H-1 NMR relaxation. *Langmuir* **2000,** 16, (7), 3030-3035.

(12) London, E.; Brown, D. A., Insolubility of lipids in Triton X-100: physical origin and relationship to sphingolipid/cholesterol membrane domains (rafts). *Biochimica Et Biophysica Acta-Biomembranes* **2000,** 1508, (1-2), 182-195.

(13) Asami, K., Dielectric properties of water in Triton X-100 (nonionic detergent)-water mixtures. *Journal of Physics-Condensed Matter* **2007,** 19, (37).

(14) Ezquerra, T. A.; Baltacalleja, F. J.; Zachmann, H. G., Real-time dielectric-relaxation of poly(ethylene-terephthalate) during crystallization from the glassy state. *Polymer* **1994,** 35, (12), 2600-2606.

(15) Mijovic, J.; Sy, J. W., Molecular dynamics during crystallization of poly(L-lactic acid) as studied by broad-band dielectric relaxation spectroscopy. *Macromolecules* **2002,** 35, (16), 6370-6376.

(16) Dionisio, M.; Viciosa, M. T.; Wang, Y. M.; Mano, J. F., Glass transition dynamics of poly(L-lactic acid) during isothermal crystallisation monitored by real-time dielectric relaxation spectroscopy measurements. *Macromolecular Rapid Communications* **2005,** 26, (17), 1423-1427.

(17) Bras, A. R.; Viciosa, M. T.; Wang, Y.; Dionisio, M.; Mano, J. F., Crystallization of poly(L-lactic acid) probed with dielectric relaxation spectroscopy. *Macromolecules* **2006,** 39, (19), 6513-6520.

(18) Laredo, E.; Grimau, M.; Barriola, P.; Bello, A.; Muller, A. J., Effect of isothermal crystallization on the amorphous phase mobility of polycarbonate/poly(epsilon-caprolactone) blends. *Polymer* **2005,** 46, (17), 6532-6542.

(19) Massalska-Arodz, M.; Williams, G.; Thomas, D. K.; Jones, W. J.; Dabrowski, R., Molecular dynamics and crystallization behavior of chiral isooctyloxycyanobiphenyl as studied by dielectric relaxation spectroscopy. *Journal of Physical Chemistry B* **1999,** 103, (20), 4197-4205.

(20) Sanz, A.; Jimenez-Ruiz, M.; Nogales, A.; Marero, D. M. Y.; Ezquerra, T. A., Hydrogen-bond network breakage as a first step to isopropanol crystallization. *Physical Review Letters* **2004,** 93, (1).

(21) Viciosa, M. T.; Correia, N. T.; Sanchez, M. S.; Carvalho, A. L.; Romao, M. J.; Ribelles, J. L. G.; Dionisio, M., Real-Time Monitoring of Molecular Dynamics of Ethylene Glycol Dimethacrylate Glass Former. *Journal of Physical Chemistry B* **2009,** 113, (43), 14209-14217.

(22) Avrami, M., Kinetics of phase change I - General theory. *Journal of Chemical Physics* **1939,** 7, (12), 1103-1112.

(23) Avrami, M., Kinetics of Phase Change. II Transformation-Time Relations for Random Distribution of Nuclei. *The Journal of Chemical Physics* **1940,** 8, (2), 212-224.

(24) Avrami, M., Granulation, Phase Change, and Microstructure - Kinetics of Phase Change. III. *Journal of Chemical Physics* **1941,** 9, (2), 177-184.

(25) Hancock, B. C.; Shamblin, S. L.; Zografi, G., MOLECULAR MOBILITY OF AMORPHOUS PHARMACEUTICAL SOLIDS BELOW THEIR GLASS-TRANSITION TEMPERATURES. *Pharmaceutical Research* **1995,** 12, (6), 799-806.
(26) Vallet-Regi, M.; Balas, F.; Arcos, D., Mesoporous materials for drug delivery. *Angewandte Chemie-International Edition* **2007,** 46, (40), 7548-7558.
(27) Angell, C. A.; Sare, J. M.; Sare, E. J., GLASS-TRANSITION TEMPERATURES FOR SIMPLE MOLECULAR LIQUIDS AND THEIR BINARY-SOLUTIONS. *Journal of Physical Chemistry* **1978,** 82, (24), 2622-2629.
(28) Farnan, I.; Stebbins, J. F., THE NATURE OF THE GLASS-TRANSITION IN A SILICA-RICH OXIDE MELT. *Science* **1994,** 265, (5176), 1206-1209.
(29) Cerveny, S.; Zinck, P.; Terrier, M.; Arrese-Igor, S.; Alegria, A.; Colmenero, J., Dynamics of Amorphous and Semicrystalline 1,4-trans-Poly(isoprene) by Dielectric Spectroscopy. *Macromolecules* **2008,** 41, (22), 8669-8676.
(30) Greer, A. L., METALLIC GLASSES. *Science* **1995,** 267, (5206), 1947-1953.
(31) Crowe, J. H.; Carpenter, J. F.; Crowe, L. M., The role of vitrification in anhydrobiosis. *Annual Review of Physiology* **1998,** 60, 73-103.
(32) Donth, E., *The Glass Transition: relaxation dynamics in liquids and disordered materials.* ed.; Springer-Verlag: Berlin, 2001.
(33) Götze, W., *Liquids, Freezing and the Glass Transition*. ed.; North-Holland: Amsterdam, 1991.
(34) Brand, R.; Lunkenheimer, P.; Loidl, A., Relaxation dynamics in plastic crystals. *Journal of Chemical Physics* **2002,** 116, (23), 10386-10401.
(35) Sousa, M. Molecular Mobility of a Liquid Crystalline Mixture in Cellulose Acetate Membranes - Evidences from a Dielectric Relaxation Spectroscopy Study. Universidade Nova de Lisboa, Lisboa, 2009.
(36) Lunkenheimer, P.; Schneider, U.; Brand, R.; Loidl, A., Glassy dynamics. *Contemporary Physics* **2000,** 41, (1), 15-36.
(37) Angell, C. A.; Ngai, K. L.; McKenna, G. B.; McMillan, P. F.; Martin, S. W., Relaxation in glassforming liquids and amorphous solids. *Journal of Applied Physics* **2000,** 88, (6), 3113-3157.
(38) Debenedetti, P. G.; Stillinger, F. H., Supercooled liquids and the glass transition. *Nature* **2001,** 410, (6825), 259-267.
(39) Viciosa, M. T. Molecular mobility of *n*-ethylene glycol dimethacrylate glass formers upon free radical polymerization. Universidade Nova de Lisboa, Lisboa, 2007.
(40) Brás, A. R. Influence of constraining an confinement in the molecular mobility of low molecular weight materials. Universidade Nova de Lisboa., Lisboa, 2009.
(41) Vogel, H., The temperature dependence law of the viscosity of fluids. *Physikalische Zeitschrift* **1921,** 22, 645-646.
(42) Fulcher, G. S., Analysis of recent measurements of the viscosity of glasses. *Journal of the American Ceramic Society* **1925,** 8, (6), 339-355.
(43) Tammann, G.; Hesse, W., The dependancy of viscosity on temperature in hypothermic liquids. *Zeitschrift Fur Anorganische Und Allgemeine Chemie* **1926,** 156, (4), 14.
(44) Kremer, F.; Schönhals, A., *Broadband Dielectric Spectroscopy*. ed.; Springer-Verlag: Berlin, 2003.
(45) Johari, G. P., INTRINSIC MOBILITY OF MOLECULAR GLASSES. *Journal of Chemical Physics* **1973,** 58, (4), 1766-1770.
(46) Adam, G.; Gibbs, J. H., ON TEMPERATURE DEPENDENCE OF COOPERATIVE RELAXATION PROPERTIES IN GLASS-FORMING LIQUIDS. *Journal of Chemical Physics* **1965,** 43, (1), 139-&.
(47) Wubbenhorst, M.; Lupascu, V., Glass transition effects in ultra-thin polymer films studied by dielectric spectroscopy - Chain confinement vs. finite size effects. *12th International Symposium on Electrets (ISE 12), Proceedings* **2005**, 87-90.
(48) Ngai, K. L., Dynamic and thermodynamic properties of glass-forming substances. *Journal of Non-Crystalline Solids* **2000,** 275, (1-2), 7-51.
(49) Johari, G. P.; Goldstei.M, VISCOUS LIQUIDS AND GLASS TRANSITION .2. SECONDARY RELAXATIONS IN GLASSES OF RIGID MOLECULES. *Journal of Chemical Physics* **1970,** 53, (6), 2372-&.
(50) Paluch, M.; Roland, C. M.; Pawlus, S.; Ziolo, J.; Ngai, K. L., Does the arrhenius temperature dependence of the Johari-Goldstein relaxation persist above T-g? *Physical Review Letters* **2003,** 91, (11).
(51) Johari, G. P., Localized molecular motions of beta-relaxation and its energy landscape. *Journal of Non-Crystalline Solids* **2002,** 307, 317-325.
(52) Ngai, K. L., Correlation between the secondary beta-relaxation time at T-g with the Kohlrausch exponent of the primary alpha relaxation or the fragility of glass-forming materials. *Physical Review E* **1998,** 57, (6), 7346-7349.

(53) Viciosa, M. T.; Rouze, N.; Dionisio, M.; Ribelles, J. L. G., Dielectric and mechanical relaxation processes in methyl acrylate/tri-ethyleneglycol dimethacrylate copolymer networks. *European Polymer Journal* **2007,** 43, (4), 1516-1529.
(54) Debenedetti, P. G., *Metastable Liquids: concepts and principles.* ed.; Princeton University Press: Princenton, 1996.
(55) Dionisio, M.; Alves, N. M.; Mano, J. F., Molecular dynamics in polymeric systems. *E-Polymers* **2004**.
(56) Schonhals, A.; Goering, H.; Schick, C.; Frick, B.; Zorn, R., Glassy dynamics of polymers confined to nanoporous glasses revealed by relaxational and scattering experiments. *European Physical Journal E* **2003,** 12, (1), 173-178.
(57) Morineau, D.; Xia, Y. D.; Alba-Simionesco, C., Finite-size and surface effects on the glass transition of liquid toluene confined in cylindrical mesopores. *Journal of Chemical Physics* **2002,** 117, (19), 8966-8972.
(58) Arndt, M.; Stannarius, R.; Gorbatschow, W.; Kremer, F., Dielectric investigations of the dynamic glass transition in nanopores. *Physical Review E* **1996,** 54, (5), 5377-5390.
(59) Arndt, M.; Stannarius, R.; Groothues, H.; Hempel, E.; Kremer, F., Length scale of cooperativity in the dynamic glass transition. *Physical Review Letters* **1997,** 79, (11), 2077-2080.
(60) Dionisio, M. Aplicação de Técnicas Dieléctricas a Estudos de Dinâmica e Estrutura Molecular. Universidade Técnica de Lisboa, Lisboa, 1993.
(61) Böttcher, C. J. F.; Bordewijk, P., *Theory of Electric Polarization*. ed.; Elsevier: Amsterdam, 1978; Vol. Vol. 2-Dielectrics in Time Dependent Fields.
(62) HP-AN1217-1, A. n., Basics of Measuring the Dielectric Properties of Materials. In ed.; 1992.
(63) Debye, P., *Polar Molecules*. ed.; Dover Publications: New York, 1945.
(64) Havrilia.S; Negami, S., A COMPLEX PLANE ANALYSIS OF ALPHA-DISPERSIONS IN SOME POLYMER SYSTEMS. *Journal of Polymer Science Part C-Polymer Symposium* **1966**, (14PC), 99-&.
(65) Havrilia.S; Negami, S., A COMPLEX PLANE REPRESENTATION OF DIELECTRIC AND MECHANICAL RELAXATION PROCESSES IN SOME POLYMERS. *Polymer* **1967,** 8, (4), 161-&.
(66) Schönhals, A.; Kremer, F., Analysis of Dielectric Spectra. In *Broadband Dielectric Spectroscopy*, Springer-Verlag: Berlin, 2003.
(67) Gao, L.; Wang, Y.; Wang, J.; Huang, L.; Shi, L.; Fan, X.; Zou, Z.; Yu, T.; Zhu, M.; Li, Z., A novel Zn-II-sensitive fluorescent chemosensor assembled within aminopropyl-functionalized mesoporous SBA-15. *Inorganic Chemistry* **2006,** 45, (17), 6844-6850.
(68) Grun, M.; Unger, K. K.; Matsumoto, A.; Tsutsumi, K., Novel pathways for the preparation of mesoporous MCM-41 materials: control of porosity and morphology. *Microporous and Mesoporous Materials* **1999,** 27, (2-3), 207-216.
(69) Merino, E. G.; Rodrigues, C.; Teresa Viciosa, M.; Melo, C.; Sotomayor, J.; Dionisio, M.; Correia, N. T., Phase Transformations Undergone by Triton X-100 Probed by Differential Scanning Calorimetry and Dielectric Relaxation Spectroscopy. *Journal of Physical Chemistry B* **2011,** 115, (43), 12336-12347.
(70) Fröhlich, H.; Clarenton Press: Oxford, *Theory of Dielectrics*. ed.; Clarendon Press: *Oxford*, 1958.
(71) Massalska-Arodz, M.; Williams, G.; Smith, I. K.; Conolly, C.; Aldridge, G. A.; Dabrowski, R., Molecular dynamics and crystallization behaviour of isopentyl cyanobiphenyl as studied by dielectric relaxation spectroscopy. *Journal of the Chemical Society-Faraday Transactions* **1998,** 94, (3), 387-394.
(72) Jensen, R. E.; O'Brien, E.; Wang, J.; Bryant, J.; Ward, T. C.; James, L. T.; Lewis, D. A., Characterization of epoxy-surfactant interactions. *Journal of Polymer Science Part B-Polymer Physics* **1998,** 36, (15), 2781-2792.
(73) Larraz, E.; Elvira, C.; San Roman, J., Novel acrylic macromonomer with amphiphilic character derived from Triton X-100: Radical copolymerization with methyl methacrylate and thermal properties. *Journal of Polymer Science Part a-Polymer Chemistry* **2003,** 41, (11), 1641-1649.
(74) Wunderlich, B., THEORY OF COLD CRYSTALLIZATION OF HIGH POLYMERS. *Journal of Chemical Physics* **1958,** 29, (6), 1395-1404.
(75) Diogo, H. P.; Ramos, J. J. M., Are crystallization and melting the reverse transformation of each other? *Journal of Chemical Education* **2006,** 83, (9), 1389-1392.
(76) Alves, N. M.; Mano, J. F.; Balaguer, E.; Duenas, J. M. M.; Ribelles, J. L. G., Glass transition and structural relaxation in semi-crystalline poly(ethylene terephthalate): a DSC study. *Polymer* **2002,** 43, (15), 4111-4122.
(77) Dias, C. J., Determination of a distribution of relaxation frequencies based on experimental relaxational data. *Physical Review B* **1996,** 53, (21), 14212-14222.
(78) Dobbertin, J.; Hannemann, J.; Schick, C.; Potter, M.; Dehne, H., Molecular dynamics of the alpha-relaxation during crystallization of a low-molecular-weight compound: A real-time dielectric spectroscopy study. *Journal of Chemical Physics* **1998,** 108, (21), 9062-9068.

(79) Andjelic, S.; Fitz, B. D., Study of reorientational dynamics during real-time crystallization of absorbable poly(p-dioxanone) by dielectric relaxation spectroscopy. *Journal of Polymer Science Part B-Polymer Physics* **2000,** 38, (18), 2436-2448.
(80) Minoguchi, A.; Nozaki, R., Broadband complex permittivity measurements of sorbitol during isothermal crystallization. *Journal of Non-Crystalline Solids* **2002,** 307, 246-251.
(81) Napolitano, S.; Wubbenhorst, M., Monitoring the cold crystallization of poly(3-hydroxy butyrate) via dielectric spectroscopy. *Journal of Non-Crystalline Solids* **2007,** 353, (47-51), 4357-4361.
(82) Avramov, I.; Avramova, K.; Russel, C., New method to analyze data on overall crystallization kinetics. *Journal of Crystal Growth* **2005,** 285, (3), 394-399.
(83) Fokin, V. M.; Schmelzer, J. W. P.; Nascimento, M. L. F.; Zanotto, E. D., Diffusion coefficients for crystal nucleation and growth in deeply undercooled glass-forming liquids. *Journal of Chemical Physics* **2007,** 126, (23).
(84) Ratta, V.; Ayambem, A.; Young, R.; McGrath, J. E.; Wilkes, G. L., Thermal stability, crystallization kinetics and morphology of a new semicrystalline polyimide based on 1,3-bis(4-aminophenoxy) benzene and 3,3 ',4,4 '-biphenyltetracarboxylic dianhydride. *Polymer* **2000,** 41, (22), 8121-8138.
(85) Pissis, P.; Kyritsis, A.; Daoukaki, D.; Barut, G.; Pelster, R.; Nimtz, G., Dielectric studies of glass transition in confined propylene glycol. *Journal of Physics-Condensed Matter* **1998,** 10, (28), 6205-6227.
(86) Barnett, S. M.; Dracheva, S.; Hendler, R. W.; Levin, I. W., Lipid-induced conformational changes of an integral membrane protein: An infrared spectroscopic study of the effects of triton X-100 treatment on the purple membrane of Halobacterium halobium ET1001. *Biochemistry* **1996,** 35, (14), 4558-4567.
(87) Bras, A. R.; Frunza, S.; Guerreiro, L.; Fonseca, I. M.; Corma, A.; Frunza, L.; Dionisio, M.; Schoenhals, A., Molecular mobility of nematic E7 confined to molecular sieves with a low filling degree. *Journal of Chemical Physics* **2010,** 132, (22).
(88) Frunza, L.; Frunza, S.; Kosslick, H.; Schoenhals, A., Phase behavior and molecular mobility of n-octylcyanobiphenyl confined to molecular sieves: Dependence on the pore size. *Physical Review E* **2008,** 78, (5).
(89) Viciosa, M. T.; Rodrigues, C.; Fernandez, S.; Matos, I.; Marques, M. M.; Duarte, M. T.; Mano, J. F.; Dionisio, M., Dielectric and thermal characterization of low density ethylene/10-undecen-1-ol copolymers prepared with nickel catalysts. *Journal of Polymer Science Part B-Polymer Physics* **2007,** 45, (19), 2802-2812.
(90) Schuller, J.; Melnichenko, Y. B.; Richert, R.; Fischer, E. W., DIELECTRIC STUDIES OF THE GLASS-TRANSITION IN POROUS-MEDIA. *Physical Review Letters* **1994,** 73, (16), 2224-2227.
(91) More information can be obtained in www.whatman.com. In ed.